Article

Cell

Regulation of the CUL3 Ubiquitin Ligase by a Calcium-Dependent Co-adaptor

Graphical Abstract

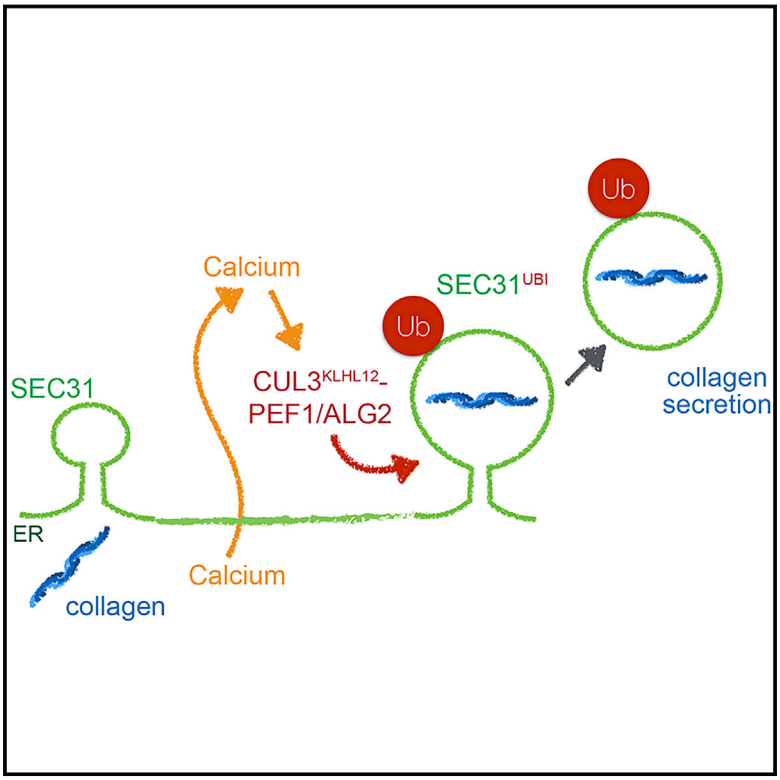

Authors

Colleen A. McGourty, David Akopian, Carolyn Walsh, ..., Randy Schekman, Diana Bautista, Michael Rape

Correspondence

mrape@berkeley.edu

In Brief

Calcium signals activate CUL3, a ubiquitin ligase that regulates neural crest specification and is linked to diseases such as autism and schizophrenia.

Highlights

- PEF1 and ALG2 are novel subunits of the CUL3^{KLHL12} ubiquitin ligase
- PEF1 and ALG2 control SEC31-ubiquitylation, COPII vesicle size, and collagen secretion
- PEF1 and ALG2 impose calcium regulation onto CUL3^{KLHL12}
- Calcium-dependent control of CUL3^{KLHL12} regulates COPII vesicle size

McGourty et al., 2016, Cell *167*, 525–538
October 6, 2016
http://dx.doi.org/10.1016/j.cell.2016.09.026

CellPress

Article

Cell

Regulation of the CUL3 Ubiquitin Ligase by a Calcium-Dependent Co-adaptor

Colleen A. McGourty,[1] David Akopian,[1,2] Carolyn Walsh,[1] Amita Gorur,[1] Achim Werner,[1] Randy Schekman,[1,2] Diana Bautista,[1] and Michael Rape[1,2,3,*]

[1]Department of Molecular and Cell Biology
[2]Howard Hughes Medical Institute
University of California, Berkeley, Berkeley, CA 94720, USA
[3]Lead Contact
*Correspondence: mrape@berkeley.edu
http://dx.doi.org/10.1016/j.cell.2016.09.026

SUMMARY

The ubiquitin ligase CUL3 is an essential regulator of neural crest specification whose aberrant activation has been linked to autism, schizophrenia, and hypertension. CUL3 exerts its roles by pairing with ~90 distinct substrate adaptors, yet how the different CUL3-complexes are activated is poorly understood. Here, we show that CUL3 and its adaptor KLHL12 require two calcium-binding proteins, PEF1 and ALG2, for recognition of their substrate SEC31. PEF1 and ALG2 form a target-specific co-adaptor that translates a transient rise in cytosolic calcium levels into more persistent SEC31 ubiquitylation, which in turn triggers formation of large COPII coats and promotes collagen secretion. As calcium also instructs chondrocyte differentiation and collagen synthesis, calcium-dependent control of $CUL3^{KLHL12}$ integrates collagen secretion into broader programs of craniofacial bone formation. Our work, therefore, identifies both calcium and CUL3 co-adaptors as important regulators of ubiquitylation events that control human development.

INTRODUCTION

Metazoan development depends on carefully executed gene expression programs that instruct pluripotent stem cells to adopt specific fates at defined times and locations within the growing organism. A failure to establish the correct sequence of differentiation events—as caused by mutations in transcription factors, loss of epigenetic regulators, or exposure to environmental toxins—can result in severe birth defects. This is illustrated by the neural crest, a collection of multipotent cells that emerge at the boundary of the neural plate and non-neural ectoderm and differentiate into various cell types, such as chondrocytes, melanocytes, or glia (Betancur et al., 2010). Mutations in genes required for neural crest specification account for more than 500 congenital diseases, and aberrant neural crest maintenance can lead to cancer, such as neuroblastoma or melanoma.

Early during development, neural crest cells migrate into the embryonic territory that is destined to become the craniofacial skeleton. These cranial neural crest cells differentiate into chondrocytes, which secrete an extracellular matrix largely composed of type II and type X collagen fibers (Karsenty et al., 2009). During the final stages of endochondral bone formation, chondrocytes are replaced by osteoblasts that produce type I collagen (Alford et al., 2015). The collagen network secreted by chondrocytes and osteoblasts provides a blueprint for the deposition of calcium-phosphate crystals that endow bones with the rigidity demanded of a major structural element of metazoan bodies (Karsenty et al., 2009). As expected from the role of collagen during bone formation, problems with neural crest specification, chondrocyte differentiation, or collagen secretion all result in aberrant craniofacial development (Twigg and Wilkie, 2015).

We recently identified the ubiquitin ligase CUL3 as a major determinant of neural crest specification and collagen secretion (Jin et al., 2012; Werner et al., 2015). CUL3 accomplishes these tasks by cooperating with distinct BTB-domain-containing substrate adaptors. When paired with KBTBD8, CUL3 monoubiquitylates the nucleolar proteins TCOF1 and NOLC1, which establishes a ribosome biogenesis platform, and $CUL3^{KBTBD8}$-dependent changes in ribosome output promote neural crest specification and chondrocyte differentiation (Werner et al., 2015). Mutations in *TCOF1* result in the craniofacial disease Treacher Collins Syndrome (Dixon and Dixon, 2004). Conversely, upon engaging its adaptor KLHL12, CUL3 monoubiquitylates the COPII coat protein SEC31 and thereby drives formation of large COPII carriers that accelerate the traffic of collagen from the endoplasmic reticulum (ER) (Jin et al., 2012). Mutations in the SEC31 interactor SEC23A prevent collagen secretion during craniofacial chondrogenesis and cause cranio-lenticulo-sutural dysplasia (Lang et al., 2006; Boyadjiev et al., 2006; Fromme et al., 2007). Underscoring their function in a shared pathway, expression of KBTBD8 and KLHL12 is co-regulated in human melanoma cells exposed to a small molecule disruptor of neural crest specification (White et al., 2011).

In addition to its role in craniofacial development, aberrant regulation of CUL3 has been associated with autism, schizophrenia, myopathy, and hypertension (De Rubeis et al., 2014; Louis-Dit-Picard et al., 2012; Ravenscroft et al., 2013). CUL3 therefore acts at multiple stages of human development and activation of specific CUL3-adaptor complexes needs to be

under tight control. This is illustrated by $CUL3^{KLHL12}$: as collagen is produced in the ER and packaged into vesicles that bud from the ER membrane (Malhotra and Erlmann, 2015), $CUL3^{KLHL12}$ has to modify its substrate SEC31 at ER exit sites, but not in the cytoplasm. The localized activation of $CUL3^{KLHL12}$ at the cytosolic face of the ER should be coordinated with the sorting of collagen into budding vesicles, an event that occurs within the ER lumen. Moreover, these reactions have to occur at the right developmental time, as premature or delayed collagen secretion result in fibrosis, fragile bones, or organismal aging (Ewald et al., 2015; Malhotra and Erlmann, 2015; Soret et al., 2015). Similar to $CUL3^{KLHL12}$, CUL3-complexes that operate in mitosis, autophagy, or endocytosis should be activated in a temporally and spatially controlled manner (Genschik et al., 2013). However, although previous studies had pointed to regulated adaptor transcription or degradation as systemic and often slow-acting means of CUL3 inhibition (Jin et al., 2012; Werner et al., 2015; Zhou et al., 2015), mechanisms that allow for rapid activation of distinct CUL3 complexes remain to be discovered. How $CUL3^{KLHL12}$ is integrated into the series of events guiding craniofacial bone formation is therefore not known.

Here, we show that the activity of $CUL3^{KLHL12}$ toward SEC31 depends on two calcium-binding proteins, PEF1 and ALG2. PEF1 and ALG2 form a target-specific co-adaptor that allows $CUL3^{KLHL12}$ to translate a transient rise in cytosolic calcium concentrations into more persistent SEC31 ubiquitylation, which drives COPII coat formation and collagen secretion. As calcium signals also instruct chondrocyte differentiation and collagen synthesis (Lin et al., 2014; Tomita et al., 2002), calcium-dependent regulation of $CUL3^{KLHL12}$ helps integrate collagen secretion into developmental programs of bone formation. We conclude that target-specific co-adaptors endow metazoan organisms with the ability to precisely tune the activity of distinct CUL3 complexes in response to developmental signals, including a rise in cytosolic calcium concentrations.

RESULTS

PEF1 and ALG2 Are Components of the $CUL3^{KLHL12}$ Ubiquitin Ligase

To discover mechanisms of CUL3 regulation, we focused on $CUL3^{KLHL12}$, which ubiquitylates SEC31 and promotes COPII coat formation and collagen secretion (Jin et al., 2012). We hypothesized that regulators of $CUL3^{KLHL12}$ might associate with KLHL12, SEC31, or both. To isolate such proteins, we affinity-purified KLHL12 from human embryonic kidney cells and used mass spectrometry to compare its interaction profile to ~150 immunoprecipitations (IPs) that used the same epitope tag, cell line, or purification procedure (Figures 1A, S1A, and S1B). Confirming earlier observations (Jin et al., 2012), these experiments found KLHL12 to efficiently bind CUL3 and SEC31. In addition, KLHL12 associated with PEF1 and ALG2, two penta-EF-hand proteins that had been reported to interact with SEC31 (Yamasaki et al., 2006; Yoshibori et al., 2012); Lunapark, which stabilizes three-way junctions in the ER (Chen et al., 2015); the BTB-domain containing CUL3 adaptor KLHL26; the ubiquitin ligase RNF219; and the KELCH-domain-directed HSP90 adaptor NUDCD3 (Taipale et al., 2014). Of these KLHL12 interactors, only PEF1 and ALG2, but not Lunapark, NUDCD3, or RNF219, were also identified in affinity purifications of SEC31 (Figures 1A and S1A).

Proteomic dissection of PEF1 and ALG2 interaction networks confirmed the association of each protein with KLHL12 and CUL3 (Figures 1A and S1A). Accordingly, both epitope-tagged and endogenous PEF1 and ALG2 precipitated with $KLHL12^{FLAG}$, as determined by immunoblot analysis (Figures 1B and 1C). These interactions also occurred at the endogenous level, and affinity purification of SEC31 revealed its binding to PEF1, ALG2, and KLHL12 (Figure 1D). Notably, the reciprocal IP of endogenous ALG2 co-depleted KLHL12 from cell lysates, which suggests that most of KLHL12 exists in complexes with ALG2 (Figure 1E).

We had previously shown that KLHL12 binds its substrate SEC31 with sufficient stability to result in co-localization of $CUL3^{KLHL12}$ and SEC31 on large COPII coats (Jin et al., 2012). By performing sequential affinity purification coupled to mass spectrometry or immunoblotting, we found that PEF1 and ALG2 remained associated with KLHL12-SEC31 complexes (Figures 2A, 2B, and S1A). Accordingly, PEF1 and ALG2, but not the alternative binding partner Lunapark, co-localized with KLHL12 and SEC31 on large COPII coats (Figures 2C, 2D, and S2A), which frequently marked compartments that contained collagen (Figure 2E). Together, these results identify PEF1 and ALG2 as components of the $CUL3^{KLHL12}$ machinery and suggest that these proteins could be involved in COPII vesicle size control and collagen secretion.

PEF1 and ALG2 Are Required for $CUL3^{KLHL12}$ Activity toward SEC31

To determine whether PEF1 and ALG2 regulate $CUL3^{KLHL12}$, we depleted each protein using small interfering RNAs (siRNAs) and tested for consequences on substrate recognition by $CUL3^{KLHL12}$. As often seen with interacting proteins, depletion of PEF1 reduced ALG2 levels and vice versa (Figure 3A). In addition, loss of PEF1 or ALG2 prevented the binding of KLHL12 or CUL3 to endogenous SEC31 (Figure 3A), which, as shown for ALG2, could be rescued by expressing a siRNA-resistant protein (see below). In a similar manner, the depletion of PEF1 or ALG2 abrogated the interaction between stably expressed KLHL12 and SEC31 without affecting the binding of KLHL12 to CUL3 (Figure S2B). Confirming the on-target effects of our siRNAs, the interaction between SEC31 and KLHL12 was also lost upon inactivation of the *PEF1* or *ALG2* genes using CRISPR/Cas9 (Figure 3B). We conclude that PEF1 and ALG2 are required in cells for the stable binding of $CUL3^{KLHL12}$ to its substrate, SEC31.

To determine whether PEF1 and ALG2 were needed for the ubiquitylation of SEC31, we expressed His-tagged ubiquitin in a cell line that allowed for inducible expression of KLHL12. We purified conjugates under denaturing conditions and then tested for ubiquitylation of endogenous SEC31 by immunoblotting. Consistent with findings using overexpressed proteins (Jin et al., 2012), induction of KLHL12 resulted in the monoubiquitylation of endogenous SEC31 (Figure 3C). $CUL3^{KLHL12}$ also catalyzed formation of some higher-molecular-weight conjugates, which likely represent SEC31 molecules ubiquitylated on multiple lysine residues (Jin et al., 2012). In contrast, if these experiments were performed in the absence of PEF1 or ALG2, $CUL3^{KLHL12}$-dependent SEC31 ubiquitylation was not observed (Figure 3C).

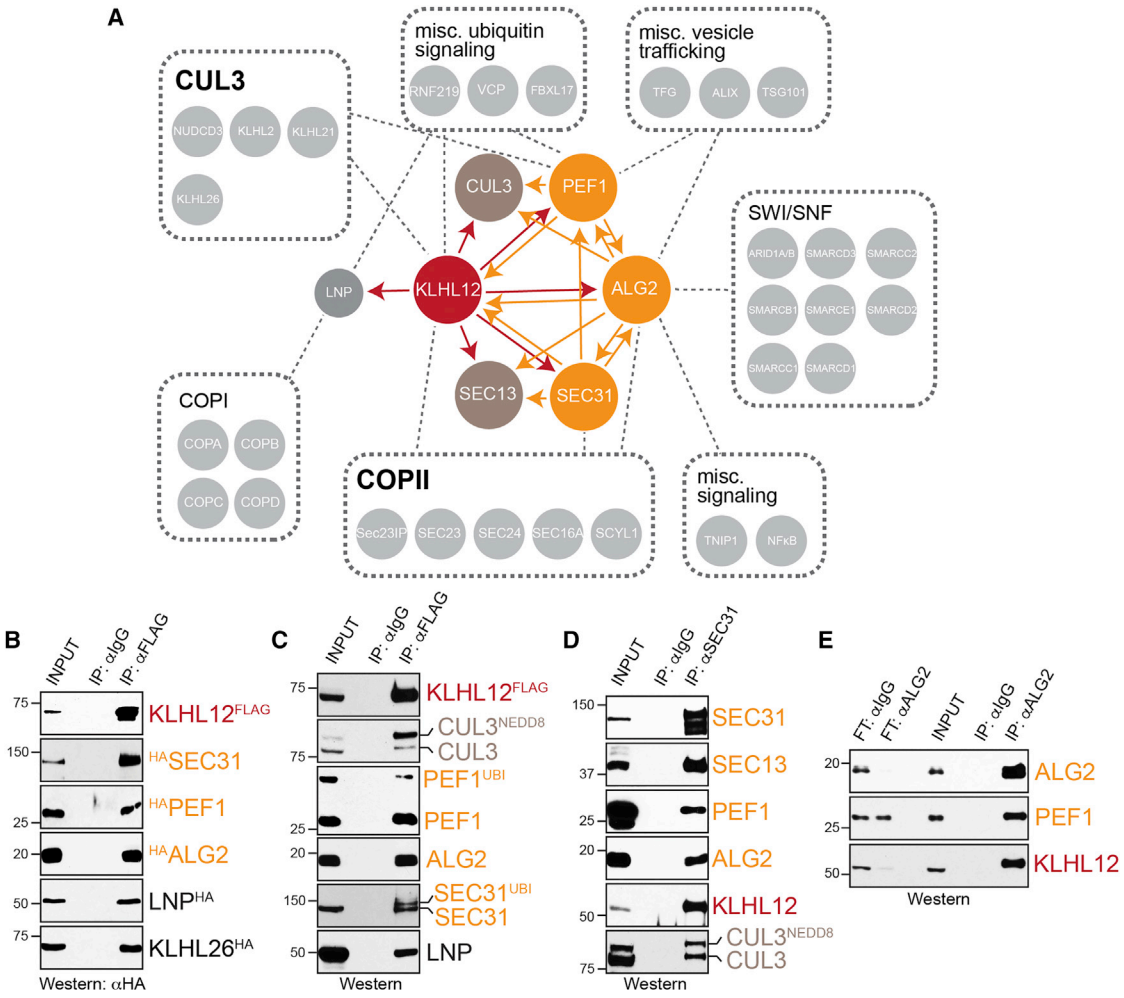

Figure 1. PEF1 and ALG2 Bind CUL3^{KLHL12}

(A) Interaction network of CUL3^{KLHL12} and SEC31. Proteins marked in red (KLHL12) or orange (PEF1, ALG2, SEC31) were used as baits for affinity purification and mass spectrometry.

(B) Validation of proteomic experiments by affinity purification coupled to immunoblotting using KLHL12^{FLAG} and HA-tagged high-confidence interactors.

(C) Validation of proteomic experiments by detecting endogenous high-confidence interactors of KLHL12^{FLAG}.

(D) Endogenous SEC31 was purified using αSEC31 antibodies, and co-precipitating proteins were detected by immunoblotting.

(E) Endogenous ALG2 was purified using αALG2 antibodies and co-precipitating PEF1 and KLHL12 were detected by immunoblotting (FT, flow-though).

See also Figure S1.

As monoubiquitylation by CUL3^{KLHL12} regulates COPII coat formation (Jin et al., 2012), we next depleted PEF1 or ALG2 from 293T cells and asked whether this treatment affected the size of COPII coats. Similar to what we had observed by confocal or electron microscopy (Jin et al., 2012), induction of KLHL12 in control cells resulted in large COPII structures that were marked by SEC31 and KLHL12 (Figures 3D, 3E, S2C, and S2D). By contrast, if cells were devoid of PEF1 or ALG2, KLHL12 did not co-localize with SEC31 and large COPII coats were not formed (Figures 3D, 3E, and S2B). The depletion of a separate KLHL12 binding partner, Lunapark, did not affect the size of COPII coats (Figure S2C), which underscores the specific requirement for PEF1 and ALG2 in these reactions.

Based on the role of large COPII vesicles in collagen transport, we finally asked whether loss of PEF1 and ALG2 affected the ER-exit of newly synthesized collagen. We first exposed human osteosarcoma cells to a heat pulse, which results in retention of pro-collagen-I in the ER, and then we shifted these cells to lower temperatures to trigger a synchronous wave of collagen export (Venditti et al., 2012). Cells treated with control siRNAs rapidly transported collagen-I from the ER to the Golgi apparatus (Figure 3F). By contrast, the loss of PEF1 or ALG2 resulted in a profound delay of collagen-I arrival at the Golgi, with many cells displaying persistent collagen ER staining throughout the time course of this experiment (Figure 3F). To investigate whether the delay in ER exit impaired collagen secretion from cells, we made use of HT1080 fibroblasts that constitutively express collagen-I, yet secrete it so efficiently that only minor collagen-I levels are detected in cell lysates (Jin et al., 2012). As expected from our other experiments, depletion of PEF1 or ALG2 from

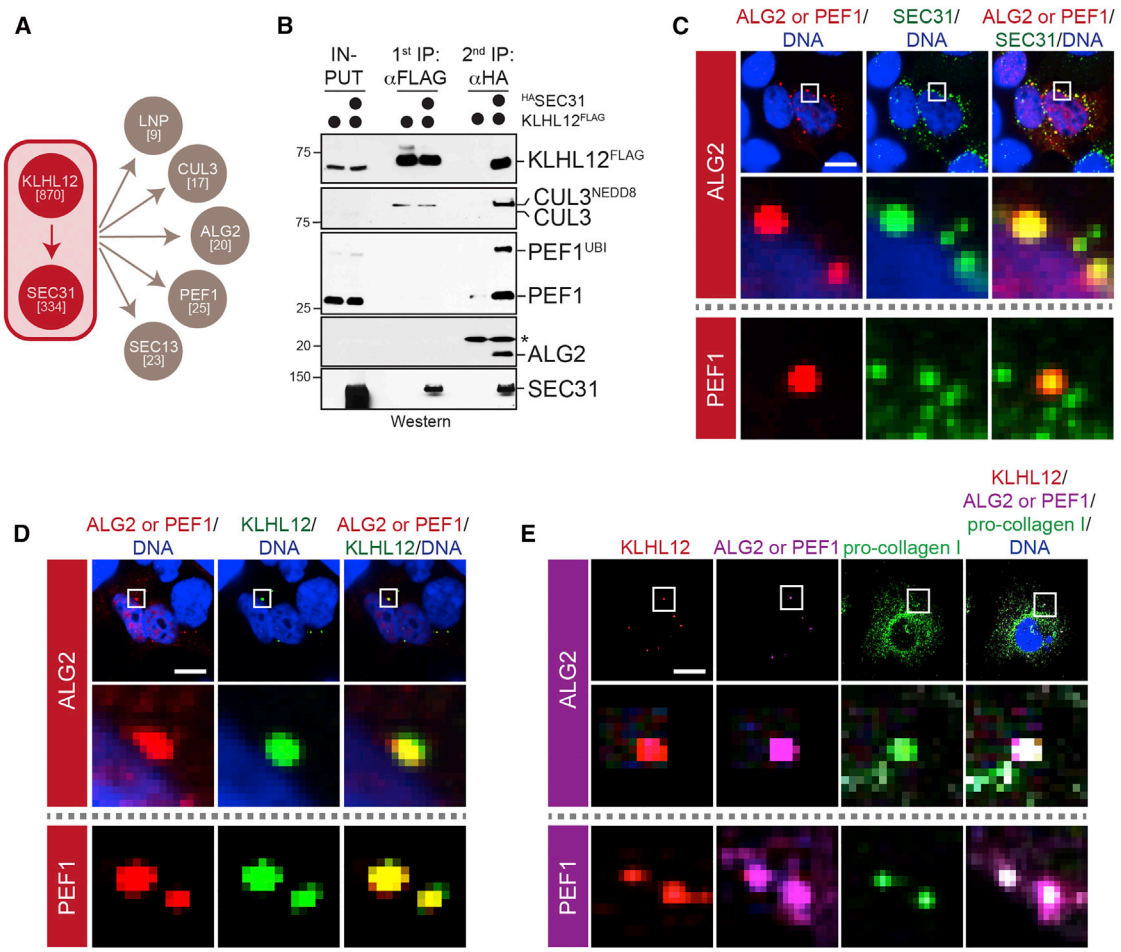

Figure 2. PEF1 and ALG2 Associate with COPII Coats

(A) Proteins bound to KLHL12-SEC31 complexes were identified by sequential affinity purification coupled to mass spectrometry.

(B) Analysis of sequential KLHL12-SEC31 purifications by immunoblot detection of endogenous high-confidence interactors.

(C) Cells expressing KLHL12 were stained for SEC31 (green), DNA (blue), and $PEF1^{HA}$ or $^{HA}ALG2$ (red, upper panels: $^{HA}ALG2$-expressing cells; panel below the dashed line: $PEF1^{HA}$-expressing cells). Scale bar, 10 μm.

(D) Cells expressing KLHL12 were stained for $KLHL12^{FLAG}$ (green), DNA (blue), and $PEF1^{HA}$ or $^{HA}ALG2$ (red, upper panels: $^{HA}ALG2$-expressing cells; panel below the dashed line: $PEF1^{HA}$-expressing cells). Scale bar, 10 μm.

(E) HT1080 cells expressing collagen-I were stained for $KLHL12^{FLAG}$ (red), $^{HA}ALG2$ or $PEF1^{HA}$ (purple), collagen-I (green) and DNA (blue, upper panels $^{HA}ALG2$-expressing cells; panel below the dashed line: $PEF1^{HA}$-expressing cells). Scale bar, 10 μm.

these cells led to a strong cellular retention of collagen (Figure 3G). Thus, PEF1 and ALG2 are required for $CUL3^{KLHL12}$ to engage SEC31, mediate SEC31 ubiquitylation, and trigger an increase in the size of COPII coats that drives collagen secretion. From these results, we infer that PEF1 and ALG2 are essential components of the $CUL3^{KLHL12}$ machinery that controls COPII vesicle size.

PEF1/ALG2 Is a Target-Specific Co-adaptor of $CUL3^{KLHL12}$

As a first step toward understanding the biochemical role of PEF1 and ALG2, we determined how these proteins engage $CUL3^{KLHL12}$ or its substrate SEC31. While analyzing the modification of SEC31, we noticed that $CUL3^{KLHL12}$ promoted the ubiquitylation of PEF1 (Figure 3C), which occurred on Lys residues in its EF-hand domain (Figure S3A). We did not observe ubiquitylation of PEF1 if cells expressed a CUL3-binding-deficient KLHL12 variant or if KLHL12 had been depleted by siRNAs (Figures S3B and S3C). As PEF1 was also modified by recombinant $CUL3^{KLHL12}$ (Figure S3D), these experiments identified PEF1 as a substrate of $CUL3^{KLHL12}$ and suggested that PEF1 might bind $CUL3^{KLHL12}$ in a manner similar to SEC31. Indeed, the same mutations in KLHL12 that blocked SEC31 ubiquitylation ($KLHL12^{FG289AA}$) (Jin et al., 2012) also prevented $CUL3^{KLHL12}$ from binding to and ubiquitylating PEF1 (Figures 4A, 4B, S3E, and S3F). Moreover, increasing concentrations of PEF1 impaired SEC31 ubiquitylation by $CUL3^{KLHL12}$ in vitro (Figure S3G) and reduced the interaction between SEC31 and KLHL12 in cells (Figure S3H). These findings indicated that PEF1 and SEC31 access an overlapping surface on the Kelch repeat of KLHL12.

Truncation analyses revealed that PEF1 binds KLHL12 through amino-terminal Gly-Pro rich repeats (Figure S4A), whereas it uses its carboxy-terminal EF-hand domain to recognize ALG2 (Figure S4B). By engaging KLHL12 and ALG2 through different motifs, PEF1 is able to bridge an interaction between $CUL3^{KLHL12}$ and ALG2 (Figure 4C). Conversely, ALG2 binds PEF1 through its fifth EF hand (Figure S4C), while it uses its first EF hand to associate with SEC31 (Figure S4D); reminiscent of PEF1, ALG2 was able to mediate an interaction between PEF1 and SEC31 (Figure 4D). Finally, SEC31, which can bind KLHL12 and ALG2 directly (Jin et al., 2012; la Cour et al., 2013), also promoted an association between these two proteins (Figure 4E). Thus, KLHL12 binds PEF1, which in turn recognizes ALG2, which associates with SEC31. The latter could finally interact with another molecule of KLHL12.

Although PEF1 and SEC31 recognize the same surface on KLHL12, different subunits of a KLHL12 dimer could contact PEF1/ALG2 and SEC31 to form the higher-order protein complex we had observed in cells (Figure 2B). Consistent with this notion, mutations that disrupt KLHL12 dimerization prevented the formation of stable $CUL3^{KLHL12}$-PEF1/ALG2-SEC31 complexes and interfered with the generation of large COPII coats (Figures 4F, S4E, and S4F). In line with these observations, we found that CUL3 was recruited to ALG2-SEC31 complexes more efficiently in the presence of PEF1 (Figure 4E), which slightly improved the in vitro ubiquitylation of SEC31 (Figure 4G). Together, these findings suggest that PEF1 and ALG2 endow $CUL3^{KLHL12}$ with an additional binding site for SEC31, which enhances the ability of $CUL3^{KLHL12}$ to recognize and ubiquitylate this particular substrate. We conclude that PEF1/ALG2 acts as a target-specific co-adaptor of $CUL3^{KLHL12}$ (Figure 4H).

PEF1/ALG2 Mediates Calcium-Dependent Substrate Recognition by $CUL3^{KLHL12}$

PEF1 and ALG2 each contain five EF hands, which could undergo conformational changes and alter their protein interactions in response to calcium binding (Clapham, 2007). Indeed, previous work had indicated that calcium stabilizes the association of ALG2 with SEC31 (la Cour et al., 2013; Takahashi et al., 2015). As $CUL3^{KLHL12}$ requires the PEF1/ALG2-complex to bind SEC31, we speculated that this E3 might read out cytosolic calcium concentrations to establish the proper timing of SEC31 ubiquitylation.

As a first test of this hypothesis, we used EGTA to chelate calcium in cell lysates and determined the consequences of this treatment on KLHL12-binding partners by quantitative tandem mass tag or semiquantitative spectral counting proteomics. In both approaches, the chelation of calcium strongly reduced the association of KLHL12 with SEC31, PEF1, and ALG2, whereas KLHL12-interactors not linked to COPII control were not affected (Figures 5A and S5A). We confirmed these observations by affinity purification of endogenous proteins coupled to immunoblot analyses (Figures 5B and 5C), as well as by reconstitution experiments: the in vitro assembly of $CUL3^{KLHL12}$-PEF1/ALG2-SEC31 complexes required at least ~130 nM calcium, with maximal complex formation observed at ~400 nM (Figures 5E–5G and S5B). The latter approach also revealed that ubiquitylation modulates the association of PEF1 with $CUL3^{KLHL12}$-SEC31: while unmodified PEF1 bound ALG2 in the absence of calcium, ubiquitylated PEF1 ($PEF1^{Ubi}$) only engaged ALG2 at calcium concentrations of ~130 nM and above (Figures 5E–5G and S5B). Thus, $CUL3^{KLHL12}$ relies on calcium to engage its key substrate SEC31.

While calcium was not required for the in vitro binding of unmodified PEF1 to KLHL12 or ALG2 (Figures 5D and S4A), its removal prevented the interaction between ALG2 and SEC31 (Figure S5C). Accordingly, chelation of calcium in cell lysates abolished the binding of ALG2 to SEC31, whereas PEF1 and $CUL3^{KLHL12}$ remained associated (Figure 6A). In line with these and previous observations (la Cour et al., 2013; Takahashi et al., 2015), mutations in the first EF hand of ALG2 that prevented calcium binding ($ALG2^{E47A}$) or calcium-dependent interactions ($ALG2^{F60A}$) also inhibited the interaction between ALG2 and SEC31 (Figures S4D and S5B). By contrast, mutating the calcium-binding site in EF hand 3 or deleting the PEF1-binding EF hand 5 of ALG2 did not affect the association between ALG2 and SEC31.

These observations implied that ALG2 has to be loaded with calcium to allow $CUL3^{KLHL12}$ to recruit SEC31. To test this hypothesis, we depleted ALG2 from embryonic kidney cells and then expressed siRNA-resistant wild-type (WT) ALG2, $ALG2^{E47A}$, $ALG2^{F60A}$, or an ALG2 variant that was unable to integrate into the $CUL3^{KLHL12}$ ligase ($ALG2^{\Delta EF5}$). As before, depletion of ALG2 abrogated the association of endogenous SEC31 with $CUL3^{KLHL12}$, which was rescued by siRNA-resistant WT ALG2 (Figure 6B). In contrast, $ALG2^{E47A}$, $ALG2^{F60A}$, or $ALG2^{\Delta EF5}$ did not reinstate recognition of SEC31 by $CUL3^{KLHL12}$ in ALG2-depleted cells (Figure 6B), and the expression of $ALG2^{E47A}$ in fact had a dominant-negative effect on the formation of KLHL12-SEC31 complexes (Figure S5D). These findings show that calcium binding to ALG2, as well as integration of ALG2 into the $CUL3^{KLHL12}$ complex, are required for $CUL3^{KLHL12}$ activation toward SEC31 in cells.

To establish whether ALG2 is sufficient to mediate the effects of calcium on substrate recognition by $CUL3^{KLHL12}$, we engineered a SEC31-ALG2 fusion that mimics a constitutive, rather than calcium-dependent, interaction between these proteins. We found that $CUL3^{KLHL12}$ was able to engage the SEC31-ALG2 fusion even in the absence of calcium (Figure 6C), which implies that formation of the SEC31-ALG2 interface is the major calcium-dependent event in $CUL3^{KLHL12}$ regulation. Interestingly, the SEC31-ALG2 fusion was polyubiquitylated, rather than monoubiquitylated (Figure 6D), which was dependent upon CUL3 (Figure S5E) and induced the proteasomal degradation of the fusion (Figure S5F). We conclude that calcium binding to ALG2 is required and sufficient for $CUL3^{KLHL12}$ to recognize its substrate SEC31 in cells. In addition to providing a mechanism of regulation, the calcium-dependent interactions of $CUL3^{KLHL12}$ ensure that SEC31 is decorated with the biologically active modification, monoubiquitylation.

A Rise in Intracellular Calcium Increases the Size of COPII Vesicles

The discovery of ALG2 as a calcium sensor for $CUL3^{KLHL12}$ allowed us to monitor CUL3 function in real time. To this end, we increased cytosolic calcium concentrations and then followed

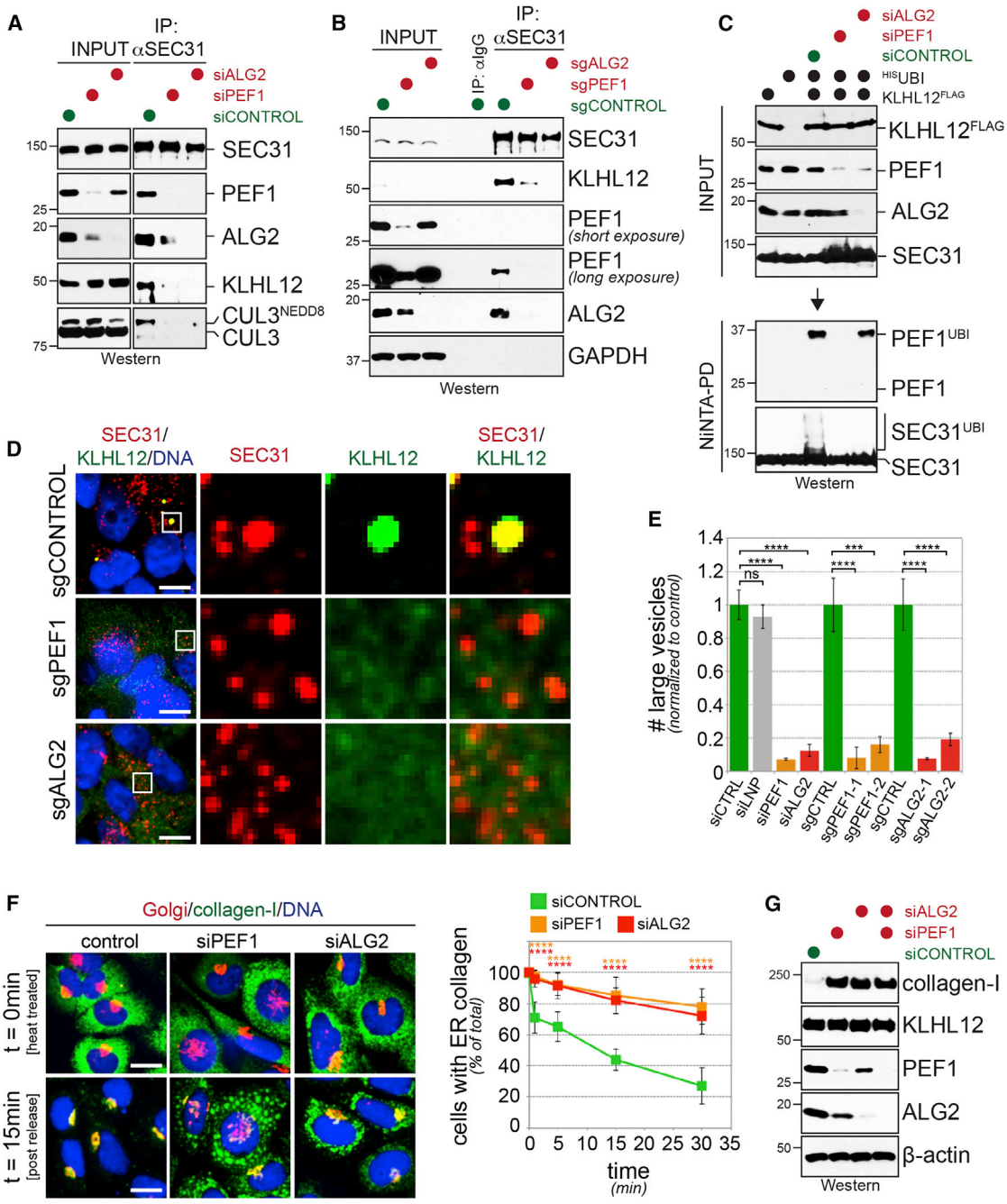

Figure 3. PEF1 and ALG2 Are Required for SEC31 Ubiquitylation by CUL3^{KLHL12}

(A) Endogenous SEC31 was affinity purified from 293T cells depleted of PEF1 or ALG2, and co-precipitating proteins were detected by immunoblotting.

(B) 293T cells were transduced with single-guide RNAs (sgRNAs) targeting *PEF1* and *ALG2*, and proteins bound to endogenous SEC31 were detected by immunoblotting.

(C) KLHL12^{FLAG} was induced in ^{HIS}ubiquitin-expressing cells, ubiquitylated proteins were purified by denaturing Nickel-nitrilotriacetic acid (NiNTA)-pull-down and analyzed by immunoblotting.

(D) Expression of KLHL12 was induced in 293T cells transduced with control sgRNAs or sgRNAs against PEF1 or ALG2. COPII coat formation was monitored by SEC31/KLHL12 co-localization using confocal microscopy. Scale bar, 10 μm.

(E) Quantification of CUL3^{KLHL12}-dependent formation of large COPII coats in the presence of different siRNAs or sgRNAs against PEF1 or ALG2. An unpaired Mann-Whitney U test was used to determine significance (***$p < 0.001$; ****$p < 0.0001$); 400–600 cells were analyzed per condition.

(legend continued on next page)

both calcium levels and stably expressed GFP-tagged ALG2 (^{GFP}ALG2). ALG2 was the only subunit of CUL3^{KLHL12} that could be labeled with GFP without compromising function. However, as the vast majority of KLHL12 was associated with ALG2 (Figure 1F), ^{GFP}ALG2 localization can serve as a proxy for CUL3^{KLHL12} activation.

We first treated IMR90 fibroblasts grown in 2 mM calcium with histamine or ionomycin to release calcium from intracellular stores followed by sustained calcium influx. Under these conditions, the global calcium concentration started at 101 ± 13 nM and peaked at 1.1 ± 0.32 μM in 11 ± 4 s. To selectively deplete calcium from intracellular stores, we treated IMR90 cells that were cultured in the absence of extracellular calcium with histamine or ionomycin. These conditions mirror physiological release of calcium from the ER and resulted in a transient increase in intracellular calcium levels (histamine: from 99.7 ± 29.4 nM to 559 ± 92.3 nM within 7.8 ± 3.2 s; ionomycin: from 91.9 ± 17.1 nM to 498 ± 117 nM within 10 ± 7.3 s).

In line with previous results (la Cour et al., 2007), the abrupt increase in calcium levels caused the re-localization of ^{GFP}ALG2 from a cytoplasmic pool to vesicular structures (Figures 7A–7C) that co-localized with SEC31 (Figure S6A). If calcium influx was permitted, the cytosolic calcium concentration reached 295.47 ± 74.5 nM in the time it took ^{GFP}ALG2 to relocate to COPII coats (τ = 5.41 ± 2.4 s; Figure 7D); this closely matched the calcium dependence of CUL3^{KLHL12}-SEC31 complex formation in vitro, which starts at 130 nM and displays saturation at ~400 nM. Similar observations were made upon depletion of intracellular calcium stores, when ^{GFP}ALG2 maximally relocated to COPII coats with a time constant of 8.75 ± 1.8 and 8.79 ± 3.5 s for histamine and ionomycin, respectively (Figures 7B and 7D). ^{GFP}ALG2 remained associated with COPII coats for the time that was required by CUL3^{KLHL12} to ubiquitylate SEC31 and PEF1 in vitro (Figure S6B). By contrast, mutating the calcium-binding site (ALG2^{E47A}), the calcium-dependent hydrophobic surface (ALG2^{F60A}), or the PEF1-binding motif that connects ALG2 to CUL3^{KLHL12} (ALG2$^{\Delta EF5}$) disrupted calcium-dependent recruitment of ALG2 to COPII vesicles (Figure 7E). These findings demonstrate that a transient rise in cytosolic calcium rapidly targets CUL3^{KLHL12}-PEF1-ALG2 to its substrate, SEC31, where it resides sufficiently long to produce the more persistent mono-ubiquitylation signal.

By controlling substrate recognition of CUL3^{KLHL12}, calcium signaling could be used to adjust COPII vesicle size if the need arises; for example, cells could recruit CUL3^{KLHL12} to budding COPII vesicles and thus promote collagen secretion in response to the high calcium levels that are encountered close to developing bones. To test this hypothesis, we increased calcium concentrations in cells that expressed KLHL12^{FLAG} and then used automated image analysis to determine whether the size of KLHL12-positive COPII structures changed in response to this treatment. Strikingly, we observed a significant increase in the average size of COPII coats and the number of large COPII vesicles within a minute of rising calcium levels (Figures 7F–7H). This regulatory circuit operated through ubiquitylation, and depletion of either CUL3 or the co-adaptor PEF1-ALG2 barred calcium from invoking an increase in the size or number of large COPII vesicles (Figure 7H). The calcium-dependent activation of CUL3^{KLHL12} therefore triggers the formation of large COPII coats that are able to initiate the process of collagen secretion.

DISCUSSION

The intricate sequence of differentiation events that establishes the human body plan relies on developmental signals being sent and received at precise times and locations within the growing organism. Akin to kinases in phosphorylation-dependent signal transduction cascades, CUL3 requires ~90 adaptors to modify its many targets, yet how distinct CUL3 complexes are turned on at the right time or place is not known. Here, we show that the ability of CUL3 and its adaptor KLHL12 to stimulate collagen secretion depends on a target-specific co-adaptor composed of PEF1 and ALG2. The PEF1/ALG2 complex allows CUL3^{KLHL12} to translate a transient rise in cytosolic calcium levels into the more persistent ubiquitylation of SEC31, which in turn triggers an increase in COPII coat size and promotes collagen secretion. Thus, in addition to identifying target-specific co-adaptors as a means for rapid CUL3 activation, our work reveals the ability of calcium signals to control specific ubiquitylation events.

Target-Specific Co-adaptors Control Substrate Recognition by CUL3

The complex between PEF1 and ALG2 endows CUL3^{KLHL12} with an additional binding site for SEC31, which is essential for SEC31 recognition, ubiquitylation, and COPII regulation in cells. This complex is anchored on CUL3^{KLHL12} by a proline-rich domain in PEF1, which occupies the same surface of CUL3^{KLHL12} as the key substrate of this E3, SEC31. Although overexpressed PEF1 may compete with SEC31 for access to KLHL12, reconstitution and sequential affinity purification showed that, at their endogenous levels, PEF1, ALG2, and SEC31 engage the same CUL3^{KLHL12} assembly. The ability of CUL3^{KLHL12} to bind both PEF1/ALG2 and SEC31 requires KLHL12 dimerization, a property that is shared with many CUL3 adaptors (Errington et al., 2012; Zhuang et al., 2009). Modification of PEF1 also contributes to these interactions, and only ubiquitylated PEF1 is able to bind CUL3^{KLHL12}-ALG2 at calcium concentrations that support formation of E3-substrate complexes in cells. We hypothesize that PEF1 ubiquitylation ensures that only active CUL3^{KLHL12} is able to engage SEC31.

(F) ER exit of collagen in heat-pulsed SaOS2 osteosarcoma cells was monitored by immunofluorescence microscopy (left) and the number of cells with ER-resident collagen-I was quantified (right). Statistical significance (****$p < 0.0001$) was determined using an unpaired Student's *t* test with >200 cells per condition; scale bar, 25 μm.

(G) HT1080 cells stably expressing collagen-I were analyzed for intracellular retention of collagen-I in the presence of control siRNAs or siRNAs against PEF1 and/or ALG2.

See also Figure S2.

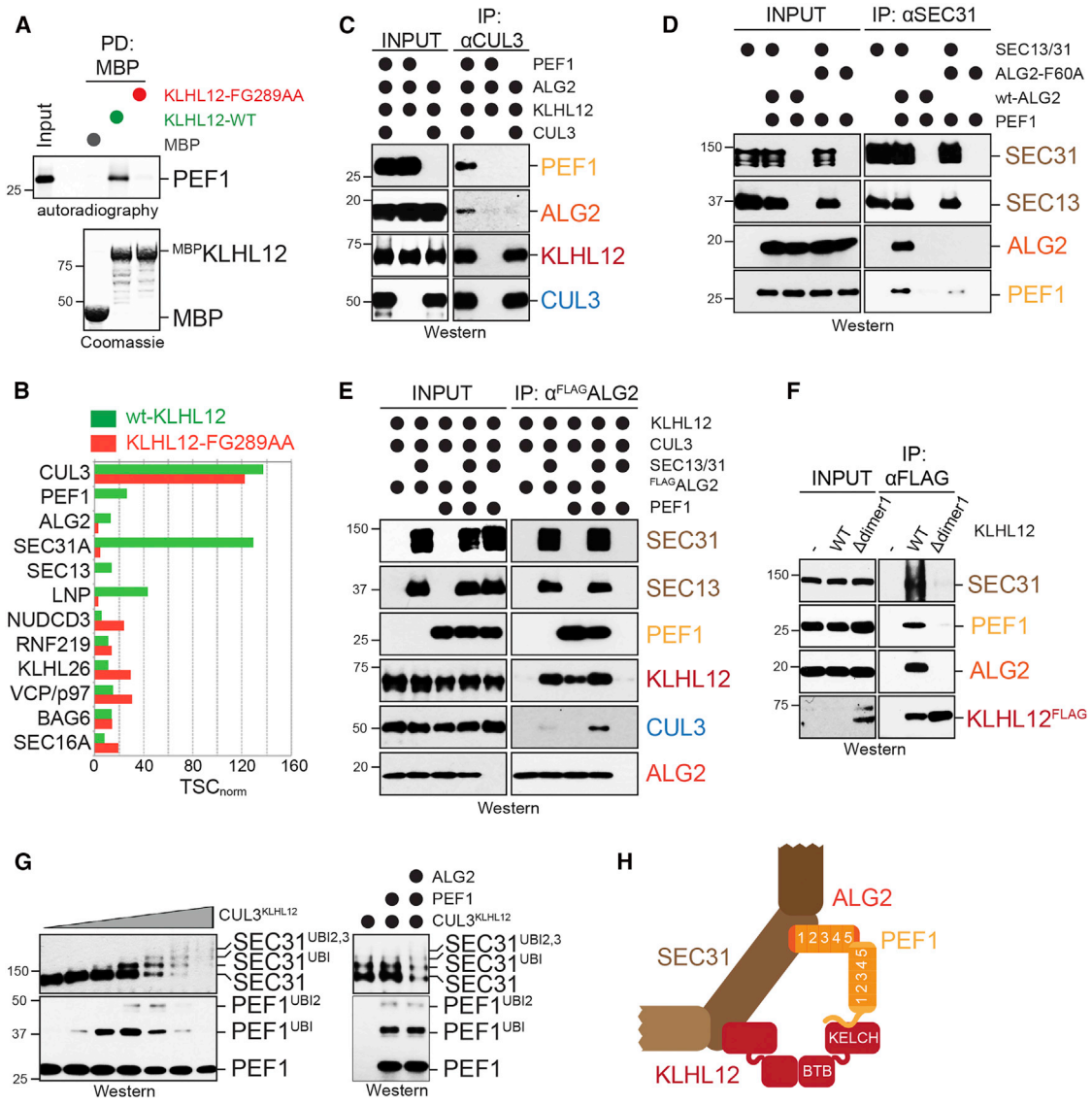

Figure 4. PEF1 and ALG2 Form a Target-Specific CUL3^{KLHL12} Co-adaptor

(A) MBP, ^{MBP}KLHL12, or ^{MBP}KLHL12^{FG289AA} were immobilized on beads and incubated with ^{35}S-labeled PEF1. Bound PEF1 was detected by autoradiography.

(B) Binding partners of affinity-purified ^{FLAG}KLHL12 or ^{FLAG}KLHL12^{FG289AA} were identified by mass spectrometry using normalized total spectral counts.

(C) Binding of recombinant ALG2 to CUL3^{KLHL12} was analyzed in the presence or absence of recombinant PEF1.

(D) Binding of recombinant PEF1 to SEC31/13 complexes was analyzed in the presence of ALG2 or ALG2^{F60A}.

(E) Binding of ALG2 to CUL3^{KLHL12} was analyzed in the presence of SEC31/13, PEF1, or both.

(F) WT or dimerization-deficient KLHL12^{FLAG} were precipitated from 293T cells and analyzed for binding to endogenous SEC31, PEF1, or ALG2.

(G) PEF1 and ALG2 slightly stimulate SEC31 ubiquitylation by CUL3^{KLHL12} in vitro. Left panel: titration of CUL3^{KLHL12} shows dose-dependent ubiquitylation and turnover of SEC31. Right panel: addition of PEF1-ALG2 complexes to CUL3^{KLHL12} ubiquitylation reactions stimulates SEC31 modification.

(H) Proposed architecture of the CUL3^{KLHL12}-PEF1-ALG2-SEC31 complex.

See also Figures S3 and S4.

Why does CUL3^{KLHL12} depend on PEF1/ALG2 in cells, even though it can directly bind and ubiquitylate SEC31 in vitro (Jin et al., 2012)? While reconstituted systems interrogate the interaction between CUL3^{KLHL12} and few substrates, more proteins could compete for recognition by CUL3^{KLHL12} in cells. This might include Dishevelled, whose ubiquitylation by CUL3^{KLHL12} induces its degradation during Wnt signaling (Angers et al., 2006), or Lunapark, an ER protein identified as a KLHL12 partner in this study. Alternatively, interactors of SEC31, such as the COPII coat component SEC23 or its abundant binding partner SEC23IP, might suppress SEC31 ubiquitylation until calcium is released from the ER to signal a need for larger COPII vesicles to transport collagen. It is also possible that SEC31 phosphorylation, which has been described in cells (Koreishi et al., 2013)

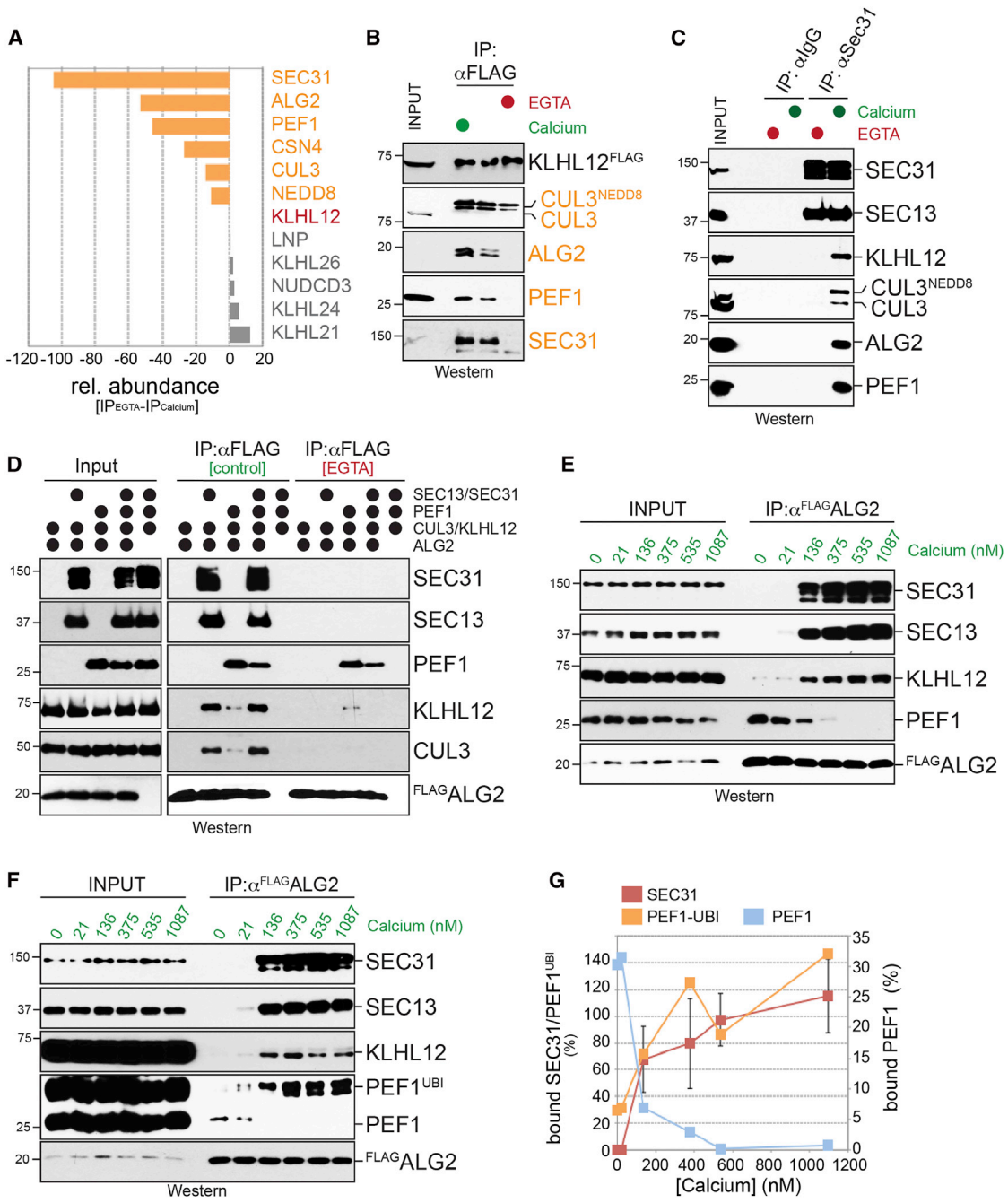

Figure 5. PEF1 and ALG2 Impose Calcium-Regulation on CUL3^{KLHL12}

(A) KLHL12^{FLAG} was purified from cell lysates treated with DMSO or EGTA, and bound proteins were quantified by tandem mass tag proteomics.

(B) KLHL12^{FLAG} was precipitated from cell lysates in the presence or absence of EGTA, and bound proteins were detected by immunoblotting.

(C) Endogenous SEC31 was purified from lysates treated with EGTA, and associated proteins were determined by immunoblotting.

(D) ^{FLAG}ALG2 was incubated with recombinant proteins either in the presence or absence of calcium, and bound proteins were detected by immunoblotting. CUL3 was expressed as a split protein, with only the 50 kD fragment being detected by the antibody.

(E) Immobilized ^{FLAG}ALG2 was incubated with indicated proteins at increasing concentrations of calcium.

(F) PEF1 was ubiquitylated in vitro by recombinant CUL3^{KLHL12}. PEF1^{UBI} and other indicated proteins were incubated with ^{FLAG}ALG2 and increasing calcium concentrations and analyzed for interactions by immunoblotting.

(G) Quantification of SEC31 binding to ALG2 (n = 3; SE of measurement), as well as of PEF1 and PEF1^{UBI} (from experiments depicted in Figures 5E and 5F). See also Figure S5.

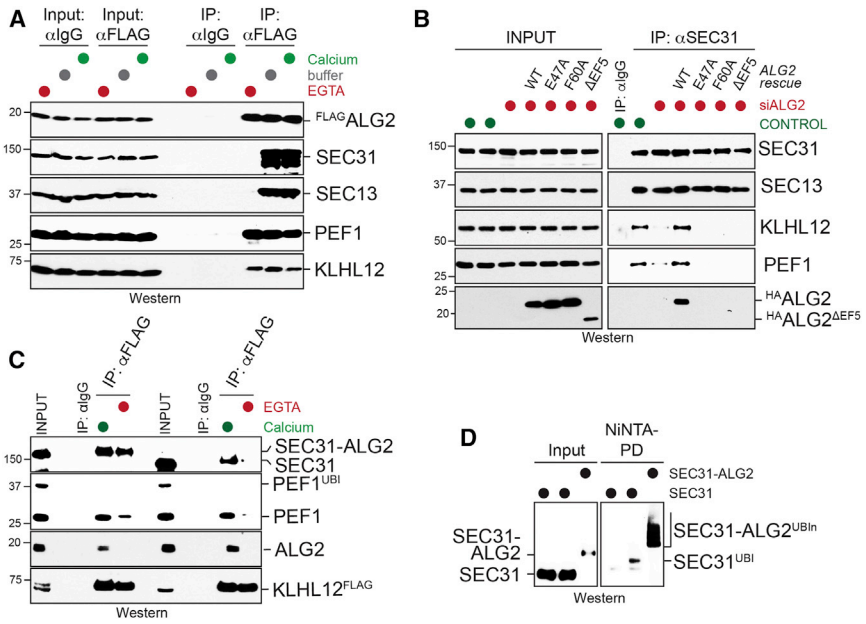

Figure 6. Calcium Binding to ALG2 Is Required and Sufficient for Substrate Recognition by CUL3^{KLHL12}

(A) ^{FLAG}ALG2 was purified from cell lysates treated with EGTA or $CaCl_2$, and bound proteins were detected by immunoblotting.

(B) Endogenous SEC31 was affinity purified from 293T cells that were depleted of ALG2 by specific siRNAs, yet expressed siRNA-resistant WT ALG2, ALG2^{E47A}, ALG2^{F60A}, or ALG2$^{\Delta EF5}$. Bound proteins were detected by immunoblotting.

(C) A fusion of SEC31 and ALG2 was purified from lysates treated with $CaCl_2$ or EGTA, and bound proteins were detected by immunoblotting.

(D) ^{HA}SEC31 or the ^{HA}SEC31-ALG2 fusion was purified from cells expressing ^{HIS}ubiquitin under denaturing conditions and analyzed for ubiquitylation by immunoblotting.

but is absent from our in vitro system, destabilizes the SEC31-KLHL12 interface to impose a requirement for PEF1 and ALG2. Independently of the mechanism, target-specific co-adaptors are most important under physiological conditions.

We anticipate that cells frequently employ target-specific co-adaptors to control CUL3 function. We recently found that CUL3^{KBTBD8}, which controls neural crest specification, requires β-arrestin for activity (Werner et al., 2015). Akin to the phenotypes of PEF1 and ALG2 depletion, loss of β-arrestin abolished the recognition and monoubiquitylation of the CUL3^{KBTBD8} substrates TCOF1 and NOLC1. As β-arrestin associates with phosphorylated peptides (Kovacs et al., 2009), it is tempting to speculate that β-arrestin acts as a target-specific co-adaptor that subjects CUL3^{KBTBD8} to phosphorylation control during neural crest specification. In addition, large-scale proteomics pointed to several CUL3 adaptors that associate with proteins enriched in interaction modules, and we believe that many of these function as co-adaptors rather than substrates (Huttlin et al., 2015). Thus, we propose that target-specific co-adaptors provide a general mechanism to control substrate recognition and ubiquitylation by variants of the CUL3 ubiquitin ligase.

Calcium-Dependent Regulation of Substrate Ubiquitylation

By rendering the recognition of SEC31 reliant on PEF1/ALG2, CUL3^{KLHL12} establishes calcium-dependent regulation of COPII coat size. Quantitative measurements of calcium concentrations revealed that the key event in this regulatory circuit, i.e., formation of the ALG2-SEC31 interface, is initiated at 130 nM calcium and occurs with maximum efficiency at ~400 nM calcium. Thus, the CUL3^{KLHL12}-PEF1-ALG2 axis is sufficiently sensitive to respond to physiological changes in cytosolic calcium levels, as they are achieved by calcium release from the ER or influx from the cell's environment (Clapham, 2007). Our microscopy experiments also showed that ALG2 is recruited to SEC31 within seconds of a rise in intracellular calcium, revealing that this machinery functions on the timescales imposed by calcium signaling.

As illustrated by the unfolded protein response (Wang and Kaufman, 2014), cells often use calcium signals to connect events that occur in the ER lumen with pathways that operate in the cytosol. In most cases, the calcium signal released from the ER dissipates on a timescale of seconds (Clapham, 2007). While this allows for enzyme regulation, as seen with CUL3^{KLHL12} or calcium-dependent kinases (Stratton et al., 2013), it is difficult to envision how such dynamic signaling directly results in large-scale cellular changes, such as those required to build a large vesicle coat. By steering an E3 ligase to its key substrate and thereby triggering the covalent modification of a coat component, cells could translate a short-lived calcium signal into a more persistent change to a cytosolic protein that is then read out by effector proteins that build large COPII coats. We therefore propose that CUL3^{KLHL12} establishes a persistent domain of COPII growth triggered by rapid calcium signaling from the ER.

While CUL3^{KLHL12} is, to our knowledge, the first E3 that requires calcium for specific substrate ubiquitylation, we expect calcium- and ubiquitin-dependent signaling to be intertwined more frequently. Indeed, E3 ligases of the RSP5/NEDD4 family contain C2 domains that bind calcium and are thought to mediate the localization of these E3s to membrane systems (Wang et al., 2010). Similar to CUL3^{KLHL12}, RSP5 performs its essential function at the ER membrane (Hoppe et al., 2000). Conversely, calcium influx into neuronal cells induces deubiquitylation of synaptic proteins (Chen et al., 2003). Together with our results, these observations point to a tight connection between calcium signaling and membrane-localized ubiquitylation events.

Coordination of Collagen Secretion and Craniofacial Bone Formation

Our work provides a potential mechanism for how cells coordinate the ER-luminal packaging of collagen into budding vesicles

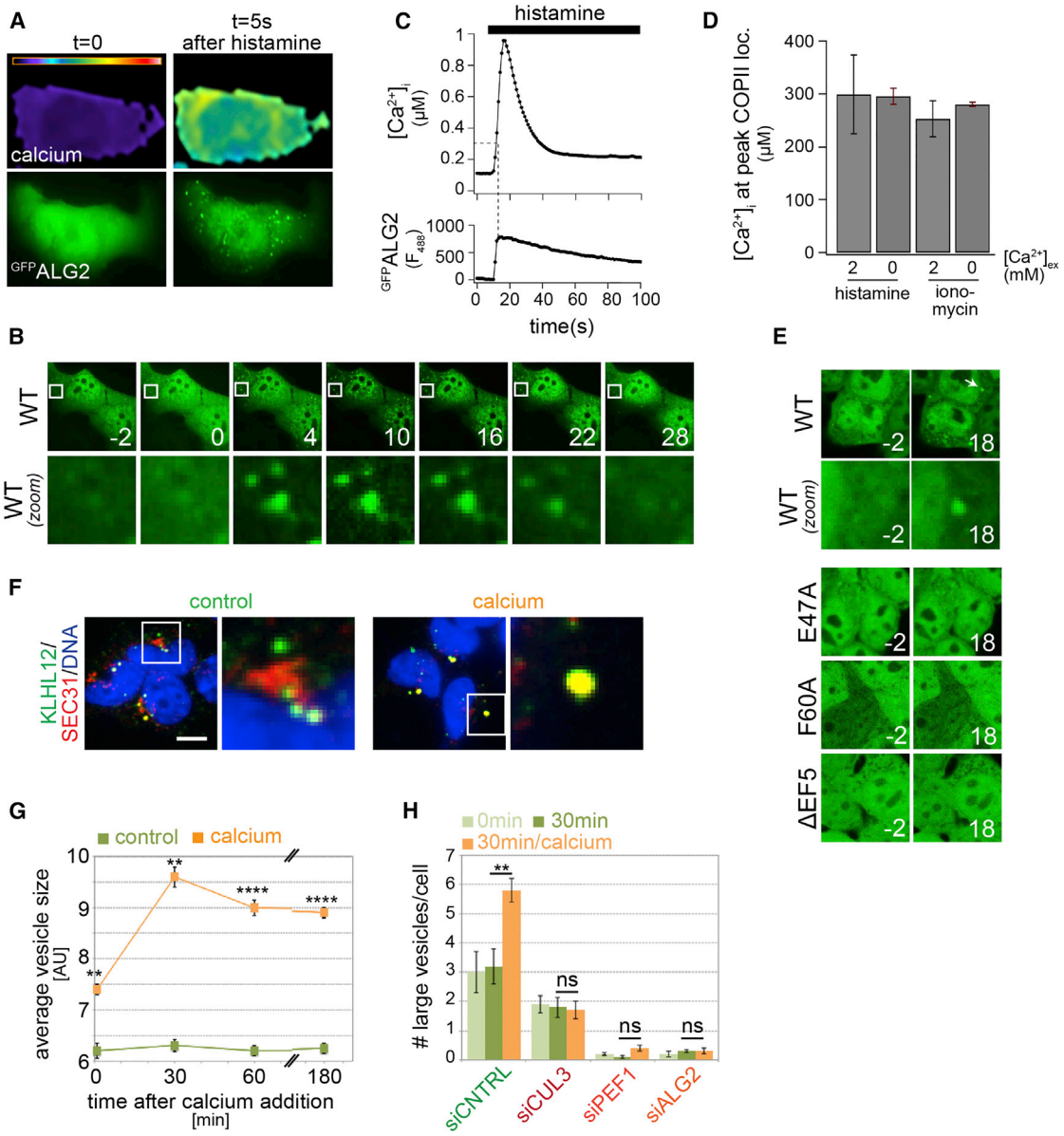

Figure 7. Regulation of CUL3^{KLHL12} Allows Calcium-Dependent Control of COPII Coat Size

(A) IMR90 fibroblasts expressing ^{GFP}ALG2 were treated with histamine (1 mM in 2 mM $[Ca^{2+}]_{EXT}$). Representative images of Fura-2-labeled and ^{GFP}ALG2-positive IMR90 cells show $[Ca^{2+}]_i$ before and 5 s after histamine application.

(B) IMR90 fibroblasts were treated with histamine, and localization of ^{GFP}ALG2 was followed by live-cell imaging.

(C) Representative traces display $[Ca^{2+}]_i$ and ^{GFP}ALG2 intensity as a function of time in a single histamine-treated cell. Maximal ^{GFP}ALG2 localization was observed within 5 s at a cytosolic calcium concentration of 295 nM.

(D) $[Ca^{2+}]_i$ measured at the peak of ^{GFP}ALG2 puncta formation in response to histamine and ionomycin in the absence and presence of extracellular calcium.

(E) Localization of ^{GFP}ALG2, ^{GFP}ALG2^{E47A}, ^{GFP}ALG2^{F60A}, and ^{GFP}ALG2$^{\Delta EF5}$ was analyzed after calcium influx by live cell imaging.

(F) 293T cells expressing KLHL12 were exposed to higher cytosolic calcium levels, and the size of KLHL12-positive COPII coats was monitored by immunofluorescence microscopy. Scale bar, 10 μm.

(G) Automated image analysis of average COPII coat size as a function of the time after calcium influx.

(H) 293T cells expressing KLHL12 were depleted of CUL3, PEF1, or ALG2. After calcium influx was triggered, the number of large KLHL12-positive vesicles was measured using automated image analysis.

See also Figure S6.

with the cytosolic regulation of COPII coat size. In this scenario, calcium channels in proximity to ER exit sites might be activated by cellular attempts to package collagen into a COPII vesicle. The ensuing release of calcium, a process implicated in the formation of calcium microdomains at the ER membrane (Petersen, 2015), could locally activate CUL3^{KLHL12} and thus allow for

ubiquitylation of those SEC31 molecules that are present at the correct location to participate in collagen trafficking. In support of this hypothesis, ALG2 not only functions as the calcium sensor of $CUL3^{KLHL12}$, but it also promotes binding of SEC31 to SEC23 (la Cour et al., 2013). SEC23 is a COPII coat component that associates with SEC24, which in turn binds to a collagen receptor, TANGO (Saito et al., 2009). To establish whether calcium signaling provides coordination between collagen sorting and coat formation, it will be important to identify the nature, localization, and regulation of any calcium transporters that participate in COPII vesicle size control and collagen secretion.

As metazoans store most of their calcium in bones, our work also suggests that $CUL3^{KLHL12}$-dependent collagen secretion is most active in cells that reside close to developing bones. Indeed, chondrocytes that are proximal to ossification centers very actively secrete collagen during bone formation (Karsenty et al., 2009). Calcium also activates a transcription factor cascade that drives chondrocyte differentiation and the transcription of collagen genes (Lin et al., 2014; Tomita et al., 2002). This role of calcium is underscored by fetal alcohol spectrum disorders, in which aberrant calcium signaling results in problems with craniofacial development (Smith et al., 2014). We propose that, by using the same signal, calcium, to activate chondrocyte differentiation, collagen synthesis, and $CUL3^{KLHL12}$-dependent collagen secretion, metazoan organisms ensure that these processes are coordinated with each other to establish robust craniofacial development.

STAR★METHODS

Detailed methods are provided in the online version of this paper and include the following:

- KEY RESOURCES TABLE
- CONTACT FOR REAGENT AND RESOURCE SHARING
- EXPERIMENTAL MODEL AND SUBJECT DETAILS
- METHOD DETAILS
  - Plasmids
  - siRNAs
  - Antibodies
  - Recombinant Proteins
  - Mammalian Cell Culture Transfections and Lentivirus Production
  - Generating CRISPR/Cas9 Knockout Cells
  - Microscopy
  - Colocalization Analysis
  - Large-scale IP-mass spectrometry and CompPASS analysis
  - Tandem Mass Tag labeling and Mass Spectrometry
  - Small-Scale IP for Western Analysis
  - Vesicle Size and Number Quantification
  - Live Cell Imaging of Calcium Responses
  - Calcium imaging
  - GFP-ALG2 live cell imaging
  - Collagen trafficking assays
  - Collagen retention assay
  - Immunofluorescence imaging of calcium responses
  - Cellular ubiquitylation assays
  - In vitro binding reactions
  - In vitro ubiquitylation assays
  - In vivo Sec31-Alg2 ubiquitylation
- QUANTIFICATION AND STATISTICAL ANALYSIS
  - KLHL12-containing vesicle number quantification (3E, 7H)
  - KLHL12-containing vesicle size quantification (7G)
  - Quantification of ER-collagen export (3F)
  - Semiquantitative analysis of MuDPIT peptides (4B, S5A)
  - Quantitation of bound SEC31, PEF1, and PEF1-UB (5E,F,G)
  - Quantification of peak ALG2-GFP puncta formation

SUPPLEMENTAL INFORMATION

Supplemental Information includes six figures and can be found with this article online at http://dx.doi.org/10.1016/j.cell.2016.09.026.

AUTHOR CONTRIBUTIONS

C.A.M., D.A., C.W., A.G., and A.W. designed, performed, and interpreted experiments; R.S., D.B., and M.R. designed and interpreted experiments; C.A.M., D.A., D.B., and M.R. wrote the paper.

ACKNOWLEDGMENTS

We are grateful to Holger Knaut, Katherine Wickliffe, and Hovik John Ashchyan for help with cloning, protein purification, and assay development. We thank Julia Schaletzky for comments on the manuscript and members of the Rape, Bautista, and Schekman labs for their help and advice. C.A.M. was funded by a predoctoral fellowship of the National Science Foundation. A.W. was a recipient of a postdoctoral fellowship by the California Institute of Regenerative Medicine. This work was in part funded by a basic biology grant of the California Institute of Medicine. M.R. and R.S. are Investigators of the Howard Hughes Medical Institute. M.R. is co-founder and consultant to Nurix, a company acting in the ubiquitin space.

Received: April 6, 2016
Revised: July 13, 2016
Accepted: September 15, 2016
Published: October 6, 2016

REFERENCES

Alford, A.I., Kozloff, K.M., and Hankenson, K.D. (2015). Extracellular matrix networks in bone remodeling. Int. J. Biochem. Cell Biol. *65*, 20–31.

Angers, S., Thorpe, C.J., Biechele, T.L., Goldenberg, S.J., Zheng, N., MacCoss, M.J., and Moon, R.T. (2006). The KLHL12-Cullin-3 ubiquitin ligase negatively regulates the Wnt-beta-catenin pathway by targeting Dishevelled for degradation. Nat. Cell Biol. *8*, 348–357.

Betancur, P., Bronner-Fraser, M., and Sauka-Spengler, T. (2010). Assembling neural crest regulatory circuits into a gene regulatory network. Annu. Rev. Cell Dev. Biol. *26*, 581–603.

Boyadjiev, S.A., Fromme, J.C., Ben, J., Chong, S.S., Nauta, C., Hur, D.J., Zhang, G., Hamamoto, S., Schekman, R., Ravazzola, M., et al. (2006). Cranio-lenticulo-sutural dysplasia is caused by a SEC23A mutation leading to abnormal endoplasmic-reticulum-to-Golgi trafficking. Nat. Genet. *38*, 1192–1197.

Chen, H., Polo, S., Di Fiore, P.P., and De Camilli, P.V. (2003). Rapid Ca2+-dependent decrease of protein ubiquitination at synapses. Proc. Natl. Acad. Sci. USA *100*, 14908–14913.

Chen, S., Desai, T., McNew, J.A., Gerard, P., Novick, P.J., and Ferro-Novick, S. (2015). Lunapark stabilizes nascent three-way junctions in the endoplasmic reticulum. Proc. Natl. Acad. Sci. USA *112*, 418–423.

Clapham, D.E. (2007). Calcium signaling. Cell *131*, 1047–1058.

De Rubeis, S., He, X., Goldberg, A.P., Poultney, C.S., Samocha, K., Cicek, A.E., Kou, Y., Liu, L., Fromer, M., Walker, S., et al.; DDD Study; Homozygosity Mapping Collaborative for Autism; UK10K Consortium (2014). Synaptic, transcriptional and chromatin genes disrupted in autism. Nature *515*, 209–215.

Dixon, J., and Dixon, M.J. (2004). Genetic background has a major effect on the penetrance and severity of craniofacial defects in mice heterozygous for the gene encoding the nucleolar protein Treacle. Dev. Dyn. *229*, 907–914.

Eletr, Z.M., Huang, D.T., Duda, D.M., Schulman, B.A., and Kuhlman, B. (2005). E2 conjugating enzymes must disengage from their E1 enzymes before E3-dependent ubiquitin and ubiquitin-like transfer. Nat. Struct. Mol. Biol. *12*, 933–934.

Errington, W.J., Khan, M.Q., Bueler, S.A., Rubinstein, J.L., Chakrabartty, A., and Privé, G.G. (2012). Adaptor protein self-assembly drives the control of a cullin-RING ubiquitin ligase. Structure *20*, 1141–1153.

Ewald, C.Y., Landis, J.N., Porter Abate, J., Murphy, C.T., and Blackwell, T.K. (2015). Dauer-independent insulin/IGF-1-signalling implicates collagen remodelling in longevity. Nature *519*, 97–101.

Fromme, J.C., Ravazzola, M., Hamamoto, S., Al-Balwi, M., Eyaid, W., Boyadjiev, S.A., Cosson, P., Schekman, R., and Orci, L. (2007). The genetic basis of a craniofacial disease provides insight into COPII coat assembly. Dev. Cell *13*, 623–634.

Genschik, P., Sumara, I., and Lechner, E. (2013). The emerging family of CULLIN3-RING ubiquitin ligases (CRL3s): cellular functions and disease implications. EMBO J. *32*, 2307–2320.

Hoppe, T., Matuschewski, K., Rape, M., Schlenker, S., Ulrich, H.D., and Jentsch, S. (2000). Activation of a membrane-bound transcription factor by regulated ubiquitin/proteasome-dependent processing. Cell *102*, 577–586.

Huttlin, E.L., Ting, L., Bruckner, R.J., Gebreab, F., Gygi, M.P., Szpyt, J., Tam, S., Zarraga, G., Colby, G., Baltier, K., et al. (2015). The BioPlex Network: A Systematic Exploration of the Human Interactome. Cell *162*, 425–440.

Jin, L., Pahuja, K.B., Wickliffe, K.E., Gorur, A., Baumgärtel, C., Schekman, R., and Rape, M. (2012). Ubiquitin-dependent regulation of COPII coat size and function. Nature *482*, 495–500.

Karsenty, G., Kronenberg, H.M., and Settembre, C. (2009). Genetic control of bone formation. Annu. Rev. Cell Dev. Biol. *25*, 629–648.

Koreishi, M., Yu, S., Oda, M., Honjo, Y., and Satoh, A. (2013). CK2 phosphorylates Sec31 and regulates ER-To-Golgi trafficking. PLoS ONE *8*, e54382.

Kovacs, J.J., Hara, M.R., Davenport, C.L., Kim, J., and Lefkowitz, R.J. (2009). Arrestin development: emerging roles for beta-arrestins in developmental signaling pathways. Dev. Cell *17*, 443–458.

la Cour, J.M., Mollerup, J., and Berchtold, M.W. (2007). ALG-2 oscillates in subcellular localization, unitemporally with calcium oscillations. Biochem. Biophys. Res. Commun. *353*, 1063–1067.

la Cour, J.M., Schindler, A.J., Berchtold, M.W., and Schekman, R. (2013). ALG-2 attenuates COPII budding in vitro and stabilizes the Sec23/Sec31A complex. PLoS ONE *8*, e75309.

Lang, M.R., Lapierre, L.A., Frotscher, M., Goldenring, J.R., and Knapik, E.W. (2006). Secretory COPII coat component Sec23a is essential for craniofacial chondrocyte maturation. Nat. Genet. *38*, 1198–1203.

Lin, S.S., Tzeng, B.H., Lee, K.R., Smith, R.J., Campbell, K.P., and Chen, C.C. (2014). Cav3.2 T-type calcium channel is required for the NFAT-dependent Sox9 expression in tracheal cartilage. Proc. Natl. Acad. Sci. USA *111*, E1990–E1998.

Louis-Dit-Picard, H., Barc, J., Trujillano, D., Miserey-Lenkei, S., Bouatia-Naji, N., Pylypenko, O., Beaurain, G., Bonnefond, A., Sand, O., Simian, C., et al. (2012). KLHL3 mutations cause familial hyperkalemic hypertension by impairing ion transport in the distal nephron. Nat. Genet. *44*, 456–460, S451–453.

Malhotra, V., and Erlmann, P. (2015). The pathway of collagen secretion. Annu. Rev. Cell Dev. Biol. *31*, 109–124.

Petersen, O.H. (2015). Ca^{2+} signalling in the endoplasmic reticulum/secretory granule microdomain. Cell Calcium *58*, 397–404.

Ravenscroft, G., Miyatake, S., Lehtokari, V.L., Todd, E.J., Vornanen, P., Yau, K.S., Hayashi, Y.K., Miyake, N., Tsurusaki, Y., Doi, H., et al. (2013). Mutations in KLHL40 are a frequent cause of severe autosomal-recessive nemaline myopathy. Am. J. Hum. Genet. *93*, 6–18.

Saito, K., Chen, M., Bard, F., Chen, S., Zhou, H., Woodley, D., Polischuk, R., Schekman, R., and Malhotra, V. (2009). TANGO1 facilitates cargo loading at endoplasmic reticulum exit sites. Cell *136*, 891–902.

Scott, D.C., Monda, J.K., Bennett, E.J., Harper, J.W., and Schulman, B.A. (2011). N-terminal acetylation acts as an avidity enhancer within an interconnected multiprotein complex. Science *334*, 674–678.

Smith, S.M., Garic, A., Berres, M.E., and Flentke, G.R. (2014). Genomic factors that shape craniofacial outcome and neural crest vulnerability in FASD. Front. Genet. *5*, 224.

Soret, R., Mennetrey, M., Bergeron, K.F., Dariel, A., Neunlist, M., Grunder, F., Faure, C., Silversides, D.W., and Pilon, N. (2015). A collagen VI-dependent pathogenic mechanism for Hirschsprung's disease. J. Clin. Invest. *125*, 4483–4496.

Sowa, M.E., Bennett, E.J., Gygi, S.P., and Harper, J.W. (2009). Defining the human deubiquitinating enzyme interaction landscape. Cell *138*, 389–403.

Stagg, S.M., Gürkan, C., Fowler, D.M., LaPointe, P., Foss, T.R., Potter, C.S., Carragher, B., and Balch, W.E. (2006). Structure of the Sec13/31 COPII coat cage. Nature *439*, 234–238.

Stratton, M.M., Chao, L.H., Schulman, H., and Kuriyan, J. (2013). Structural studies on the regulation of Ca2+/calmodulin dependent protein kinase II. Curr. Opin. Struct. Biol. *23*, 292–301.

Taipale, M., Tucker, G., Peng, J., Krykbaeva, I., Lin, Z.Y., Larsen, B., Choi, H., Berger, B., Gingras, A.C., and Lindquist, S. (2014). A quantitative chaperone interaction network reveals the architecture of cellular protein homeostasis pathways. Cell *158*, 434–448.

Takahashi, T., Kojima, K., Zhang, W., Sasaki, K., Ito, M., Suzuki, H., Kawasaki, M., Wakatsuki, S., Takahara, T., Shibata, H., and Maki, M. (2015). Structural analysis of the complex between penta-EF-hand ALG-2 protein and Sec31A peptide reveals a novel target recognition mechanism of ALG-2. Int. J. Mol. Sci. *16*, 3677–3699.

Tomita, M., Reinhold, M.I., Molkentin, J.D., and Naski, M.C. (2002). Calcineurin and NFAT4 induce chondrogenesis. J. Biol. Chem. *277*, 42214–42218.

Twigg, S.R., and Wilkie, A.O. (2015). New insights into craniofacial malformations. Hum. Mol. Genet. *24* (R1), R50–R59.

Venditti, R., Scanu, T., Santoro, M., Di Tullio, G., Spaar, A., Gaibisso, R., Beznoussenko, G.V., Mironov, A.A., Mironov, A., Jr., Zelante, L., et al. (2012). Sedlin controls the ER export of procollagen by regulating the Sar1 cycle. Science *337*, 1668–1672.

Wang, M., and Kaufman, R.J. (2014). The impact of the endoplasmic reticulum protein-folding environment on cancer development. Nat. Rev. Cancer *14*, 581–597.

Wang, J., Peng, Q., Lin, Q., Childress, C., Carey, D., and Yang, W. (2010). Calcium activates Nedd4 E3 ubiquitin ligases by releasing the C2 domain-mediated auto-inhibition. J. Biol. Chem. *285*, 12279–12288.

Werner, A., Iwasaki, S., McGourty, C.A., Medina-Ruiz, S., Teerikorpi, N., Fedrigo, I., Ingolia, N.T., and Rape, M. (2015). Cell-fate determination by ubiquitin-dependent regulation of translation. Nature *525*, 523–527.

White, R.M., Cech, J., Ratanasirintrawoot, S., Lin, C.Y., Rahl, P.B., Burke, C.J., Langdon, E., Tomlinson, M.L., Mosher, J., Kaufman, C., et al. (2011). DHODH modulates transcriptional elongation in the neural crest and melanoma. Nature *471*, 518–522.

Wickliffe, K.E., Lorenz, S., Wemmer, D.E., Kuriyan, J., and Rape, M. (2011). The mechanism of linkage-specific ubiquitin chain elongation by a single-subunit E2. Cell *144*, 769–781.

Wilson, S.R., Gerhold, K.A., Bifolck-Fisher, A., Liu, Q., Patel, K.N., Dong, X., and Bautista, D.M. (2011). TRPA1 is required for histamine-independent, Mas-related G protein-coupled receptor-mediated itch. Nat. Neurosci. *14*, 595–602.

Yamasaki, A., Tani, K., Yamamoto, A., Kitamura, N., and Komada, M. (2006). The Ca2+-binding protein ALG-2 is recruited to endoplasmic reticulum exit sites by Sec31A and stabilizes the localization of Sec31A. Mol. Biol. Cell *17*, 4876–4887.

Yoshibori, M., Yorimitsu, T., and Sato, K. (2012). Involvement of the penta-EF-hand protein Pef1p in the Ca2+-dependent regulation of COPII subunit assembly in Saccharomyces cerevisiae. PLoS ONE *7*, e40765.

Zhou, Z., Xu, C., Chen, P., Liu, C., Pang, S., Yao, X., and Zhang, Q. (2015). Stability of HIB-Cul3 E3 ligase adaptor HIB Is Regulated by Self-degradation and Availability of Its Substrates. Sci. Rep. *5*, 12709.

Zhuang, M., Calabrese, M.F., Liu, J., Waddell, M.B., Nourse, A., Hammel, M., Miller, D.J., Walden, H., Duda, D.M., Seyedin, S.N., et al. (2009). Structures of SPOP-substrate complexes: insights into molecular architectures of BTB-Cul3 ubiquitin ligases. Mol. Cell *36*, 39–50.

STAR★METHODS

KEY RESOURCES TABLE

REAGENT or RESOURCE	SOURCE	IDENTIFIER
Antibodies		
Mouse monoclonal anti-KLHL12 clone 2G2	Cell Signaling Technology	Cat#9406
Chicken polyclonal anti-KLHL12	Novus	Cat#NB120-14233; RRID: AB_788263
Mouse monoclonal anti-Sec31A	BD	Cat#612350; RRID: AB_399716
Mouse monoclonal anti-Sec31A	Santa Cruz	Cat#sc-376587; RRID: AB_11151395
Rabbit monoclonal anti-PEF1/peflin	Abcam	Cat#ab137127
Mouse monoclonal anti-pro-collagen I	QED	Cat#42024; RRID: AB_215361
Rabbit anti-pro-collagen I, LF-41	Larry Fisher, NIH	N/A
Rabbit polyclonal anti-ALG2/PDCD6	Proteintech	Cat#12303-1-AP; RRID: AB_2162459
Rabbit polyclonal anti-Lunapark	Abcam	Cat#ab121416; RRID: AB_11129552
Chemicals, Peptides, and Recombinant Proteins		
UbcH5	Eletr et al., 2005	N/A
KLHL12	Jin et al., 2012	N/A
CUL3/RBX1	Expression plasmid from Brenda Schulman	N/A
APPBP1/UBA3 (Nedd8 E1)	Eletr et al., 2005	N/A
^{6xHisFLAG}ALG2	This paper	N/A
^{6xHis}Sec31A/Sec13	Stagg et al., 2006	N/A
Ube2M	Scott et al., 2011	N/A
Ubiquitin E1	Wickliffe et al., 2011	N/A
PEF1	This paper	N/A
Nedd8	Boston Biochem	Cat#UL-812
Ubiquitin	Boston Biochem	Cat#U-100H
Histamine	Sigma Aldrich	Cat#H7250
Ionomycin	Sigma Aldrich	Cat#I0634
Fura-2AM	ThermoFisher	Cat#F1201
Fura Red-AM	ThermoFisher	Cat#F3020
Pluronic F-127	ThermoFisher	Cat#P6867
EGTA	Sigma-Aldrich	Cat#E8145
Doxycycline hyclate	Sigma-Aldrich	Cat#D9891
L-Ascorbic Acid	Sigma-Aldrich	Cat#255564
L-ascorbic acid 2-phosphate	Sigma-Aldrich	Cat#A8960
cycloheximide	Sigma-Aldrich	Cat#239764
3x-flag peptide	Sigma-Aldrich	Cat#F4799
Protein A/G fusion magnetic beads	ThermoFisher	Cat#88803
TMTduplex Isobaric Label Reagent 2-plex set	ThermoFisher	Cat#90063
Experimental Models: Cell Lines		
HEK293T	ATCC	Cat#CRL-3216; RRID: CVCL_0063
Saos-2	ATCC	Cat#HTB-85; RRID: CVCL_0548
293Trex Tet-inducible KLHL12-3xflag	Jin et al., 2012	N/A
HT-1080 expressing stable pro-collagen I (HTPC 1.1)	Jin et al., 2012	N/A
SV-40 immortalized IMR90	UC Berkeley Cell Culture Facility	N/A
Recombinant DNA		
KLHL12-FLAG pCS2+ (wild-type, FG289AA, LSE67AAA, and L20D/M23D/L26D/I49K)	This paper	N/A

(*Continued on next page*)

Continued

REAGENT or RESOURCE	SOURCE	IDENTIFIER
PEF1-FLAG pCS2+	This paper	N/A
Lunapark-FLAG pCS2+	This paper	N/A
KLHL12-HA pCS2+ (wild-type, FG289AA, LSE67AAA, and L20D/M23D/L26D/I49K)	This paper	N/A
HA Sec31A pCS2+		N/A
HA-ALG2 pCS2+	This paper	N/A
HA-PEF1 pCS2+ (wild-type, K137R/K165R/K167R, and all K→R)	This paper	N/A
RFP-Sec31A pRK5	This paper	N/A
HA-Sec31/ALG2 fusion pCS2+	This paper	N/A
HA-ALG2 pEF-EntrA (wild-type, E47A, E114A, F60A, ΔEF5)	This paper	N/A
FLAG-ALG2 pEF-EntrA (wild-type, E47A, E114A, F60A, ΔEF5)	This paper	N/A
GFP-ALG2 pEF-EntrA (wild-type, E47A, E114A, F60A, ΔEF5)	This paper	N/A
pLentiX1 (puromycin resistance)	Eric Campeau via Addgene	Plasmid# 17297
LentiCRISPR v2	Feng Zheng via Addgene	Plasmid# 52961
LentiCRISPR v2 targeting PEF1: cloned using author's instructions against GGAGCTGCAGGACAAGCACC	This paper	N/A
LentiCRISPR v2 targeting ALG2: cloned using author's instructions against GAACTCGCTGAAGTTCACGC	This paper	N/A
^{His6FLAG}ALG2 pET30a (wild-type, E47A, E114A, F60A, ΔEF5)	This paper	N/A
MBP-KLHL12^{His6} pET28	Jin et al., 2012	N/A
^{His6}Sec31A pFastbac1	Randy Schekman, HHMI/UC Berkeley	N/A
Sec13-HA pFastbac1	Randy Schekman, HHMI/UC Berkeley	N/A
^{His6}MBP-PEF1 pFastbac1	This paper	N/A
Sequence-Based Reagents		
Control siRNA oligo: UAGCGACUAAACACAUCAAUU	GE Dharmacon	N/A
siRNA oligo targeting human ALG2 3′-UTR: CAUUGUGCCA UGAGGUAAAUU	This paper	N/A
siRNA oligo targeting human PEF1 3′-UTR: GGUCCUUGUA AUGGAGUUAUU	This paper	N/A
siRNA Smart Pool targeting human KLHL12	GE Dharmacon	L-015890-00-0005
siRNA Smart Pool targeting human Lunapark	GE Dharmacon	L-023148-01-0005
Software and Algorithms		
Metamorph Advanced	Molecular Devices	RRID: SCR_002368
GraphPad Prism	GraphPad Software, Inc.	RRID: SCR_002798
MetaFluor	Molecular Devices	RRID: SCR_014294
Igor Pro	WaveMetrics	RRID: SCR_000325
ImageJ (https://imagej.nih.gov/ij/index.html)	N/A	RRID: SCR_003070

CONTACT FOR REAGENT AND RESOURCE SHARING

Michael Rape, Howard Hughes Medical Institute (HHMI) and University of California, Berkeley, mrape@berkeley.edu.

EXPERIMENTAL MODEL AND SUBJECT DETAILS

The following human cell lines were used in this study, the sources of which are indicated in the key resources table: HEK293T; Saos2; 293Trex with stably integrated doxycycline-inducible KLHL12-3xFLAG; HT1080 with stably integrate pro-collagen I; SV40-immortalized IMR90 cells;

Human embryonic kidney (HEK) 293T, Saos2, and IMR90 cells were maintained in DMEM with 10% fetal bovine serum. HEK293T cells expressing doxycycline-inducible KLHL12^{3xFLAG} were grown in DMEM with certified Tet- fetal bovine serum. HT1080 cells

expressing pro-collagen I and doxycycline-inducible KLHL12$^{3x\ FLAG}$ were grown in DMEM with 10% Tet- FBS with non-essential amino acids. Cells were periodically tested for mycoplasma contamination.

METHOD DETAILS

Plasmids

For transient expression in human cells and in vitro transcription/translation, the following constructs were cloned into pCS2+: KLHL12^{FLAG}, PEF1^{FLAG}, KLHL12^{HA}, PEF1^{HA}, ^{HA}Sec31, ^{HA}ALG2, Lunapark^{HA}, ^{6xHIS}Ubiquitin, dominant-negative CUL3 (residues 1-450), PEF1 N terminus (residues 1-109) PEF1 C terminus (residues 109-284). Sec31A was cloned into RFP-pRK5 (a gift from Rosalie Lawrence and Roberto Zoncu, UC Berkeley). Sec31A-ALG2 fusion constructs were generated by simultaneously ligating ^{HA}-Sec31A and ALG2 inserts with complementary restriction sites into pCS2+.

For stable expression, ^{HA}ALG2, ^{FLAG}ALG2, and ^{GFP}ALG2 and corresponding mutants were cloned into pEF-EntrA and recombined into pLentiX1-puro using Gateway LR clonase II (Invitrogen).

For expression in Sf9 ES insect cell expression, ^{His6x}Sec31A, ^{HA}Sec13, and ^{6xHis}MBP-Tev-PEF1 were cloned into pFastbac1 then recombined using the bac-to-bac baculovirus expression system (Invitrogen). ^{6xHisFLAG}ALG2 was cloned into pET30 for expression in *Escherichia coli.*

The following mutations were introduced into multiple vectors using site-directed mutagenesis of parental DNA followed by DpnI digestion: ALG2 E47A, E114A, F60A, and ΔEF5, PEF1 K137R, K165R, and K167R, KLHL12 FG289AA, LSE67AAA, and L20D/M23D/L26D/I49K).

CRISPR/Cas9 guides were designed using the MIT CRISPR design tool and cloned into pLentiCRISPR v2 (a gift from Feng Zheng, addgene #52961). The sequences are as follows: PEF1 targeting, (GGAGCTGCAGGACAAGCACC), and ALG2 targeting, (GAACTCGCTGAAGTTCACGC), and non-targeting guide. Bacterial expression plasmids CUL3 purification and Nedd8 E1 (APPBP1-Uba3) were provided by Brenda Schulman (HHMI, St. Jude's Childrens Research Hospital).

siRNAs

The following siRNA oligos were purchased from Dharmacon: Scrambled control (UAGCGACUAAACACAUCAAUU), PEF1 3′-UTR (GGUCCUUGUAAUGGAGUUAUU) ALG2 3′-UTR (CAUUGUGCCAUGAGGUAAAUU), KLHL12 SMARTpool (GGAAGGUGCCGG ACUCGUAUU, GCAGGGAUCUGGUUGAUGAUU, GGACUAAUGUUACACCAAUUU, UGACAAAUACUCAUGCUAAUU), Lunapark SMARTpool (GAAACUUACAAGACGGCUAUU, GUGUUUACAUUAAGCGGUAUU, ACGAUGUUCUUGAUGAUAAUU, GUGGAACA GUUAAGUAGAAUU).

Antibodies

The following antibodies were used: KLHL12 (Cell Signaling, 9406, mouse monoclonal), KLHL12 (Novus, NB120-14233, chicken polyclonal), SEC31 (BD, 612350, mouse monoclonal), Sec31 (Santa Cruz, sc-376587, mouse monoclonal), PEF1/peflin (Abcam, ab137127, rabbit monoclonal), ALG2/PDCD6 (Proteintech, 12303-1-AP, rabbit polyclonal), CUL3 (Bethyl, A301-109A, rabbit polyclonal), Lunapark (Abcam, ab121416, rabbit polyclonal), pro-collagen I (QED, 42024, mouse monoclonal), GM130 (Abcam, ab52649 rabbit monoclonal) HA (Cell Signaling, C29F4, rabbit monoclonal), FLAG (Sigma, F7425, rabbit polyclonal,), β-actin (MP Biomedicals, clone 4, mouse monoclonal), GAPDH (Cell Signaling 14C10, rabbit monoclonal), α-tubulin (Calbiochem, DM1A, mouse monoclonal). SEC13 rabbit polyclonal antibody was a gift from Randy Schekman at University of California Berkeley/HHMI. Goat-anti-Mouse Alexa488 and Goat-anti-Rabbit Alexa568 (Invitrogen), Donkey-anti-Chicken IgY Fluorescien (Jackson Immunoresearch), HRP Goat-anti-Mouse IgG light-chain specific (Jackson Immunoresearch), HRP Goat-anti-Mouse IgG (Sigma), and HRP Goat-anti-Rabbit IgG (Sigma) were used as secondary antibodies.

Recombinant Proteins

UbcH5, KLHL12, CUL3, and Nedd8 E1 were expressed and purified from BL21/DE3 (RIL) cells as described (Eletr et al., 2005; Jin et al., 2012). ^{6xHisFLAG}ALG2 was cloned into pET30 and grown to LB medium to OD^{600nm} 0.8 and induced with 0.5mM IPTG (Lab Scientific, Inc.) at 37°C for 3h. Cells were harvested at lysed by sonication in 20mM Tris (pH 8.0), 150mM NaCl with protease inhibitor tablets (Roche). Imidazole was added to 10mM and lysate was incubated with NiNTA resin (QIAGEN) for 2h at 4°C, and eluted in 20mM Tris (pH 8.0), 150mM NaCl, 300mM imidazole. Protein was diluted to 50 μM and dialyzed overnight into 20mM Tris (pH 8.0), 150mM NaCal, 1mM DTT.

^{6xHis}Sec31A/Sec13 complex, Ube2M, and E1 were purified from Sf9 cells as described (Scott et al., 2011; Stagg et al., 2006; Wickliffe et al., 2011). PEF1 was also purified from Sf9 cells: 6xHisMBP-TEV-PEF1 was cloned into pFastbac1, packaged into baculovirus, and expressed in Sf9 cells for 72h. Cells were collected and lysed by sonication in 50mM Tris (pH 8.0), 150mM NaCl, and 10% glycerol with protease inhibitor. Imidazole was added to 10mM and lysate was incubated with NiNTA resin for 2h at 4°C. ^{6xHis}MBP-TEV-PEF1 was eluted with 50mM Tris (pH 8.0), 150mM NaCl, 10% glycerol, and 300mM imidazole. Protein was dialyzed overnight into 50mM Tris (pH 8.0), 150mM NaCl, and 10% glycerol. To obtain MBP-tagged protein, dialyzed protein at this step was used. To obtain untagged protein, dialyzed ^{6xHis}MBP-TEV-PEF1 was incubated overnight with ^{6xHis}TEV protease at 4°C. Cleaved ^{6xHis}MBP and ^{6xHis}TEV were removed by incubating with NiNTA resin.

Mammalian Cell Culture Transfections and Lentivirus Production

Plasmid transfections of HEK293T cells were with calcium phosphate or lipofectamine 2000 according to the manufacturers instructions, and siRNA transfections were with Lipofectamine RNAiMAX (Invitrogen) using 20nM for each siRNA.

Lentiviruses were produced in 293T cells by co-transfection of lentiviral constructs with packaging plasmids (Addgene) for 48–72h. Viruses were collected and filtered through a 0.45 μm filter and stored at −80°C. Cells were transduced in polybrene (6 μg/ml) and selected in puromycin (Sigma, 0.5-2 μg/ml) until cell death was complete (2-7d).

Generating CRISPR/Cas9 Knockout Cells

293T cells were transduced with lentiviruses containing Cas9 and sgRNA expression constructs (LentiCRISPR v2) and selected using puromycin for 7d. After selection, the degree of editing of the bulk cell population was determined by western blot for PEF1 and ALG2.

Microscopy

For immunofluorescence, cells were seeded on poly-d-lysine coated coverslips. Cells were fixed for 10min in 4% paraformaldehyde in PBS and washed three times in PBS. Cells were permeabilized in PBS with 0.1% Triton X-100 for 10 min and blocked for 30min in PBS with 5% normal donkey serum. Cells were stained in primary antibody diluted in PBS for 2h at room temperature, washed 4 times in PBS, and incubated with fluorescent secondary antibodies and Hoechst (AnaSpec Inc.) for 45min at room temperature covered in foil. Coverslips were washed 4 times in PBS then mounted on glass slides using Pro-long gold antifade reagent (Life Technologies). For live cell imaging, cells were seeded on glass-bottom Lab-tek imaging chambers. Images were acquired on a Zeiss LSM 710 confocal microscope using 40X, 60X, and 100X oil objectives.

Colocalization Analysis

For colocalization studies, cells were transfected with HA- and FLAG- tagged constructs for 24 hr. After staining, cells were imaged using a 60x objective, and Z-stacks were obtained at 0.5 μm thickness imaging while imaging 3 colors at each confocal plane. Colocalization was determined by analyzing single planes.

Large-scale IP-mass spectrometry and CompPASS analysis

αFLAG IPs for mass spectrometry analysis were performed from extracts of HEK293T cells transiently or virally expressing 1x-FLAG versions of KLHL12, Sec31A, PEF1, ALG2, and Lunapark (20 × 15cm dishes per condition). Cells were lysed in 2 pellet volumes of 50mM HEPES (pH 7.5), 1.5 mM MgCl2, 5mM KCl and 0.1% Triton X-100 by freeze/thaw in liquid nitrogen and multiple passages through a 25G5/8 needle. Debris was pelleted by centrifugation at 21000G for 1h, and lysates were passed through a 0.22 μm filter for further clearing, then NaCl concentration was increased to 150mM. Under Ca^{2+} chelation conditions, EGTA was added at this step and in all future buffers to 5mM. Lysates were incubated with 100 μl of αFLAG-M2 agarose resin (Sigma) for 2 hr at 4°C, then beads were washed 5 times in cold 50mM HEPES (pH 7.5), 150mM NaCl,1.5 mM $MgCl_2$, 5mM KCl and 0.1% Triton X-100. Proteins were eluted in 3 incubation steps at 30°C each with 250 μl of 3xFLAG peptide (0.5mg/ml in PBS). For sequential IPs, eluates were further incubated 100 μl anti-HA-resin (SIGMA) for 2h at 4°C, washed 5 times as described above at eluted with 3xHA peptide (Biosynthesis). Eluates were processed for multi-dimensional protein identification technology (MuDPIT). CompPASS analysis was performed as described (Huttlin et al., 2015; Sowa et al., 2009).

Tandem Mass Tag labeling and Mass Spectrometry

Samples were prepared in the same manner as MuDPIT mass spectrometry experiments described above. After trypsin digestion, samples were desalted using a C18 spec tip (Agilent A57203) and dried on a speed vacuum overnight. Peptides were resuspended in 80 μl 200mM HEPPS pH 8.0 and quantified using Pierce Quantitative Colorimetric Peptide Assay Kit (Pierce 23275) using a microplate reader per manufacturer's instructions. Peptides were normalized to equal masses in 100 μl volumes using 200mM HEPPS pH 8.0. TMT labeling was performed using TMTduplex Isobaric Label Reagent 2-plex set (ThermoFisher 90063) per manufacturer's instructions. Labeled samples were combined in equal volumes and desalted and dried as described previously. Mass spectrometry was performed by the Vincent J. Coates Proteomics Mass Spec Laboratory at UC Berkeley using a Lumos Orbitrap mass spectrometer.

Small-Scale IP for Western Analysis

Cells were collected and lysates were obtained as described above, with the exception of the 0.22 μm filtration step, which was not performed for small-scale experiments. For FLAG IPs, lysates were incubated for 2h at 4°C with 15 μl of αFLAG-M2 agarose, washed 5 times in cold HEPES (pH 7.5), 150mM NaCl,1.5 mM $MgCl_2$, 5mM KCl and 0.1% Triton X-100. For endogenous IPs, lysates were incubated for 2h at 4°C with 3 μg of primary antibody, then coupled to 15 μl Protein A/G fusion magnetic beads (ThermoFisher, #88803). Beads were washed 4 times and proteins were eluted in 2x sample buffer (25% glycerol, 3% SDS, 50mM Tris pH 6.8, 5% β-mercaptoethanol).

Vesicle Size and Number Quantification

Doxycycline-inducible 293T::$KLHL12^{FLAG}$ cells were reverse-transfected with 20nM siRNA using Lipofectamine RNAiMAX and incubated for 48h on poly-lysine coated coverslips. Expression of $KLHL12^{FLAG}$ was induced by treatment with doxycycline (1 μg/mL) for

12h. To assess knockout cells, Control, PEF1, and ALG2 CRISPR-Cas9 knockout cells were treated similarly. Cells were fixed for 10min in paraformaldehyde (4% in PBS) and processed for immunofluorescence. 3D Confocal images were obtained using a 60x objective at a 0.5 μm thickness. $KLHL12^{FLAG}$-positive vesicles were defined by setting a pre-determined FLAG signal brightness threshold and using this to create 3D binary Z-stack images using Metamorph. Vesicle number and size in each plane were then assessed using the ImageJ particle analysis plugin. To obtain vesicle number, particles were counted then normalized to the number of nuclei in each image to account for differences in cell density. To assess response to Ca^{2+} influx, cells were processed as described above but treated for indicated amounts of time with ionomycin (3 μM) in Ringers buffer. Three biological replicates were performed and at least 400 cells were analyzed per condition. When analyzing vesicle size, over 2000 individual vesicles were analyzed. A Mann-Whitney U-test was applied to each experiment to determine significance.

Live Cell Imaging of Calcium Responses

Human embryonic kidney (HEK) 293T cells or IMR90 cells were infected with lentiviruses to express GFP-ALG2 WT and mutants. After 3 days, cells were seeded onto 8-well imaging chambers (Lab-Tek). For two-color movies, cells were transfected for 12hrs with RFP-Sec31A using lipofectamine 2000. Prior to imaging, cells were washed 2 times with Ringer's buffer or Ringer's buffer containing 10mM EGTA. Buffer was removed immediately prior to imaging and replaced with corresponding Ringer's buffers with DMSO, 3 μM ionomycin (Sigma), or 10 μM histamine (Sigma).

Calcium imaging

Ca^{2+} imaging experiments were carried out as previously described (Wilson et al., 2011). Cells were loaded for 30min with 5 μM Fura-2AM, supplemented with 0.01% Pluronic F-127 (wt/vol, Life Technologies), in physiological Ringer's solution (in mM) 140 NaCl, 5 KCl, 10 HEPES, 2 $CaCl_2$, 2 $MgCl_2$ and 10 D-(+)-glucose, pH 7.4. EGTA Ringer's solution contained: (in mM) 140 NaCl, 5 KCl, 10 HEPES, 10 EGTA 10 D-(+)-glucose, pH 7.4. Background subtracted F_{340} and F_{380} images were collected every second and analyzed using MetaFluor (Molecular Devices). Intracellular calcium concentration was determined from background-corrected F_{340}/F_{380} ratio images using the relation $[Ca^{2+}]_i = K^*(R-R_{min})/(R_{max}-R)$ with the following parameters that we measured via in situ *calibration in each of the following cell types: 1)* HEK293t cells: R_{min} = 0.27; R_{max} = 6.2; K^* = 1.1μM; and 2) IMR90 cells: R_{min} = 0.12; R_{max} = 4.1; K^* = 1.43μM Image analysis and statistics were performed using custom routines in Igor Pro (WaveMetrics).

GFP-ALG2 live cell imaging

Human embryonic kidney (HEK) 293T cells or IMR90 cells were infected with lentiviruses to express GFP-ALG2 WT and mutants. After 3 days, cells were seeded onto 8-well imaging chambers (Lab-Tek). For two-color movies, cells were transfected for 12hrs with RFP-Sec31A using lipofectamine 2000 F_{488} and F_{584} Images were collected once/second before and after perfusing cells with Ringer's containing 1 μM ionomycin (Sigma), or 10 μM histamine (Sigma). Images were analyzed using Metamorph (Molecular Devices).

Collagen trafficking assays

Saos-2 cells were reverse transfected with siRNAs (20nM) and seeded onto coverslips in a 6-well dish. After 48h, cells were incubated for 3h at 40°C. After incubation, media was removed and replaced with DMEM with 10% fetal bovine serum, ascorbate (50 μg/ml) and cycloheximide (50 μg/ml) and temperature-shifted to 32°C. At indicated times, cells were fixed in 4% paraformaldehyde in PBS and processed for immunofluorescence.

Collagen retention assay

HT1080 cells expressing procollagen I and containing doxycycline-inducible KLHL12 were seeded into 35mm dishes at 150,000 cells per dish and reverse transfected with 20nM siRNAs targeting ALG2, PEF1, or both. 24h post-transfection, the medium was replaced with fresh DMEM/FBS and 20h later, the cells were induced with 2 μg/mL doxycycline. The cells were harvested 12h post-induction, washed once with sterile PBS, and trypsinized. Trypsin was quenched with DMEM/FBS, the cells were spun down and washed once with sterile PBS. The washed cells were resuspended in 2X Laemmli/6M urea lysis buffer, sonicated, heated to 65°C, and the concentration of the total protein was determined by means of Pierce 660 protein assay. Equal amounts of total protein were resolved on SDS gel and analyzed by western blotting for intracellular collagen.

Immunofluorescence imaging of calcium responses

293T cells expressing doxycycline-inducible KLHL12 were seeded on poly-lysine coated coverslips and reverse-transfected with siRNAs (20nM) when applicable. Prior to treatment, cells were washed twice with Ringer's buffer then incubated in Ringer's buffer with DMSO or 3 μM ionomycin. Cells were fixed and processed for immunofluorescence.

Cellular ubiquitylation assays

For detection of SEC31A and PEF1 ubiquitylation, HEK293T cells were transfected with ^{6xHis}Ubiquitin and $KLHL12^{FLAG}$. To determine the effect of PEF1 and ALG2 depletion, cells with transfected with PEF1 and ALG2 siRNAs 24hrs before plasmid transfection. Cells were harvested washed with PBS, lysed in Urea lysis buffer (ULB) (8M urea, 300 mM NaCl, 0.5% NP40, 50 mM Na_2HPO_4, 50 mM

Tris-HCl pH 8) and sonicated. ^{6xHis}Ubiquitin conjugates were purified by incubation and rotation with NiNTA agarose for 1h at room temperature. Beads were washed 5x with ULB supplemented with 10mM imidazole. Ubiquitin conjugated were eluted in sample buffer and ubiquitylated proteins were detected by western blot.

In vitro binding reactions

In vitro binding assays were performed at room temperature in binding buffer (150mM NaCl, 50mM KHEPES, pH 7.5, 3mg/mL BSA, 10% glycerol, 0.05% TWEEN, EDTA-free protease inhibitor tablets) supplemented either with 1mM EGTA or increasing CaCl2 concentrations (determined by fluorescence-based calcium imaging using Fura-2 ratiometric calcium-binding dye). Recombinant $^{6xHis-FLAG}$ALG2, PEF1, KLHL12, CUL3/RBX1 (1 μM each) and 0.5 μM SEC31 were mixed in the binding buffer and incubated at room temperature for 1h. The mixture was incubated with M2 anti-FLAG affinity resin (10 μl) with mixing for 2h in a total volume of 90 μl. The beads were washed six times with binding buffer and eluted with FLAG peptide in a total volume of 90 μl by incubating at 30°C with mixing. 80 μl of the eluted protein solution was mixed with 3X Laemmli buffer and heated for 5min at 95°C. The elution mixture was resolved on a denaturing gel and the protein levels were assayed by western blotting. Similar experiments were performed to interrogate the association between ^{6xHisFLAG}ALG2 mutants (10 μg) and SEC31/13 complexes, only that binding was assessed by SDS-PAGE and Coomassie staining.

PEF1 full-length, N-terminal domain, and C-terminal domain were synthesized from pCS2+ vectors by in vitro transcription-translation in rabbit reticulocyte lysate (Promega). 1 μg of DNA was combined with 20 μl of rabbit reticulocyte lysate and 3 μl of ^{35}S-labeled cysteine/methione mixture (Perkin Elmer). Reactions were incubated at 30°C for 2h. 10 μg ^{MBP}KLHL12 (wt and FG289AA) was coupled to 20ul amylose resin (New England Biociences) in 50mM HEPES (pH 7.5), 150mM NaCl, 1.5 mM $MgCl_2$, 5mM KCl and 0.1% Tween20 for 1.5 hr rotating at 4°C. Beads were washed 3 times in the same buffer, then 5 μl in vitro translated PEF1 constructs were added. Reactions were incubated at 4°C for 2h, then washed 4 times. Proteins were eluted in sample buffer and detected by Coomassie and autoradiography of SDS-PAGE gels.

In vitro ubiquitylation assays

Ubiquitylation of SEC31 and PEF1 was performed using a modified reconstituted system as previously described (Jin et al., 2012). 5 μM Cul3/Rbx1 was neddylated in the presence of 63 μM Nedd8, 0.7 μM E1, 0.8 μM Ube2M, and energy regenerating system in 1X UBA buffer (50mM Tris-HCl pH 7.5, 50mM NaCl, 10mM $MgCl_2$) at 30°C for 7min. Recombinant KLHL12 was added to neddylated Cul3/Rbx1 and diluted to 200nM Cul3/Rbx1, 330nM KLHL12). The ligase dilutions were mixed with the reaction mixture containing recombinant 50nM SEC31, 50nM PEF1, saturating ubiquitin, E1, UBCH5, energy regenerating system, and 1mM DTT in 1X UBA buffer. The reaction were carried out for 1h at 30°C and quenched with 2X Laemmli/6M urea. The samples were heated at 65°C and analyzed by western blotting. If ubiquitylation of SEC31 was interrogated in the presence of PEF1 and ALG2, 50nM SEC31 was supplemented with 150nM PEF1 and 150nM ALG2. The reactions were performed for 1 hr at 30°C and processed as described above. Competition between PEF1 and SEC31 ubiquitylation was assayed using 50nM SEC31 and increasing concentrations of Pef1 (0, 260, 520, 1040, 3420nM) and assayed in the presence of saturating ligase (550nM Cul3/Rbx1 and 1.59 μM KLHL12).

In vivo Sec31-Alg2 ubiquitylation

HEK293T cells allowing for doxycycline inducible KLHL12 expression were transfected at 60% confluence with plasmids encoding ^{HIS6}ubiquitin, SEC13, ^{HA}SEC31 or the SEC31-ALG2 fusion using polyethyleneimine. 24h post-transfection, the cells were treated with 2 μg/mL doxycycline and harversted 30h later. Cells were washed and the cell pellet was resuspened in 2mL of Urea lysis buffer (ULB) (8M urea, 300mM NaCl, 0.5% NP40, 50mM Na_2HPO_4, 50mM Tris-HCl, pH 8) and incubated on a rotary shaker for 20min. The samples were lysed by sonication, centrifuged at 15,000rpm, 15min, and the lysates were normalized for protein concentrations and adjusted to 2mL using ULB. Lysates were supplemented with 10mM imidazole, mixed with 300 μl of Ni-NTA agarose, and incubated on a rotary shaker at room temperature for 1.5h. The resin was washed five times with 5mL per wash of ULB/10mM imidazole. The final wash was removed completely and the resin was resuspended in 250 μl of 1X Laemmli buffer containing 300mM imidazole. The samples were incubated at 65°C with mixing for 10min, resolved on 10% and 5% denaturing gels, and analyzed by western blotting. The CUL3-dependence of the SEC31-ALG2 fusion ubiquitylation was tested in cells co-transfected with dominant-negative CUL3 (residues 1-252). The cells were treated and the samples processed as described above.

QUANTIFICATION AND STATISTICAL ANALYSIS

KLHL12-containing vesicle number quantification (3E, 7H)

KLHL12^{FLAG}-containing vesicles were defined by setting a pre-determined FLAG signal brightness threshold and using this to create 3D binary Z-stack images using Metamorph. Vesicles and nuclei were then counted using the particle analysis plugin in ImageJ. This number was then normalized to the number of nuclei in each image. This analysis was performed on three biological replicates per condition (siRNA, sgRNA) and a total of 400-600 cells per condition were analyzed. Error bars indicating the standard error of measurement (SEM) are shown in Figure 3E. Significance was determined using an unpaired Mann-Whitney U-test in GraphPad Prism. Significance values are indicated in Figure 3E, &H with **$p < 0.01$; ***$p < 0.001$; ****$p < 0.0001$.

KLHL12-containing vesicle size quantification (7G)

KLHL12FLAG-containing vesicles were defined as described for Figures 3E and 7H. A size measurement in pixels was determined using the ImageJ particle analysis plugin. The average vesicles size was calculated from measurements of at least 2000 individual vesicles over three biological replicates. The SEM of each time point and condition was calculated and is indicated within the figure. Significance was determined using an unpaired Mann-Whitney U-test is GraphPad Prism. Significance values are indicated within the figure (**$p < 0.01$; ***$p < 0.001$; ****$p < 0.0001$).

Quantification of ER-collagen export (3F)

Collagen-I localization was determined by co-staining for the *cis*-Golgi marker GM130. File names were blinded and collagen-I localization to either ER or Golgi was determined by sight. Experiment was performed in three replicates and 200 cells per replicate per time point were analyzed. SD of each condition and time point are indicated in Figure 3F, and significance was determined using a Student's *t* test ($p < 0.001$; ****$p < 0.0001$).

Semiquantitative analysis of MuDPIT peptides (4B, S5A)

Total spectral counts (TSC) were normalized such that the TSCs of bait peptides for each experiment were set to 100, and interacting protein TSCs were adjusted based on their abundance relative to bait peptides. ΔTSC_{norm} was calculated by subtracting normalized interactor peptides between the two indicated experimental conditions.

Quantitation of bound SEC31, PEF1, and PEF1-UB (5E,F,G)

Calcium dependent FLAG-ALG2 pull-down of SEC31, PEF1, and PEF1-UB was quantitated using ImageJ software (NIH). The intensity (integrated area) of the highest intensity band of the six bands in the INPUT lanes and the ELUTION lanes was set to 1 and the intensities of the five remaining bands were represented as a fraction relative to 1. The ratio of the ELUTION band intensity to the INPUT band intensity at every calcium concentration was converted to % and represents % protein bound. The error bars represent SD.

Quantification of peak ALG2-GFP puncta formation

Image analysis was performed using MetaFluor software. To quantitate fluorescence intensities of puncta, images were thresholded, and data from pixels above the threshold were quantified. The time to peak puncta fluorescence after addition of histamine was performed using custom routines in IgorPro (WaveMetrics).

Supplemental Figures

A

bait: / binder:	KLHL12 (1644)	SEC31 (5461)	PEF1 (472)	ALG2 (524)	LNP (395)	KLHL12/ SEC31/
KLHL12		17	131	11	41	870
SEC31	210			419		345
PEF1	43	13		263		25
ALG2	22	11	29			20
LNP	71					9
Ub	62	8	191	26	17	26
CUL3	225	4	94	94	24	17
SEC13	23	566		148		23
SEC16A	14		14	89	16	89
NUDCD3	10		11		3	
FBXL17	20		6			
RNF219	20				28	
KLHL26	19		10			3
CUL1	10					
BAG6	28		7			
SEC23B	3	8				
SEC23A	4	25	4	2		
SCYL1		377				
SEC23IP		439		82		
SEC24C		38			6	
SEC24D		6				
P4HB			152			
P4HA1			109	33		
PPM1A			31			
FASN			77		89	
ARIH1			13			
SMARCB1				58		
PDCD6IP				687		
DPF2				53		
HEBP2				307		
SMARCD1				58		
TFG				30	6	
SMARCC1				181		
KCTD15				15		
NFkB p105				56		
ARID1A				153		
TNIP1				22		
SMARCE1				48		
CHERP				49		
TSG101				13		
FAM125A				13		
SMARCC2				63		
ARID1B				43		
SMARCA2				56		
SEC24B				9		
VCP					81	
COPA					59	
COPB					22	
COPC					33	
COPD					12	
COPB					22	

B

	transient	transient	viral	viral	stable
KLHL12	1262	1644	793	384	2070
SEC31	145	210	186	44	426
SEC13	11	23	23	11	38
PEF1	39	43	26	12	151
ALG2	17	22	46	11	394
CUL3	220	210	186	44	572
LNP	28	71	24	9	25

(legend on next page)

Figure S1. Interaction Network of the CUL3^{KLHL12} Ubiquitin Ligase, Related to Figure 1

(A) High-confidence interactors of KLHL12, SEC31, PEF1, and ALG2 were determined by affinity purification coupled to CompPASS mass spectrometry. Peptide counts for high-confidence interactors are shown. The last column shows the results of a sequential affinity purification of KLHL12-SEC31 complexes.

(B) Representative KLHL12 interactors detected in five independent KLHL12^{FLAG} affinity purifications. The blue bar denotes the method of KLHL12 expression.

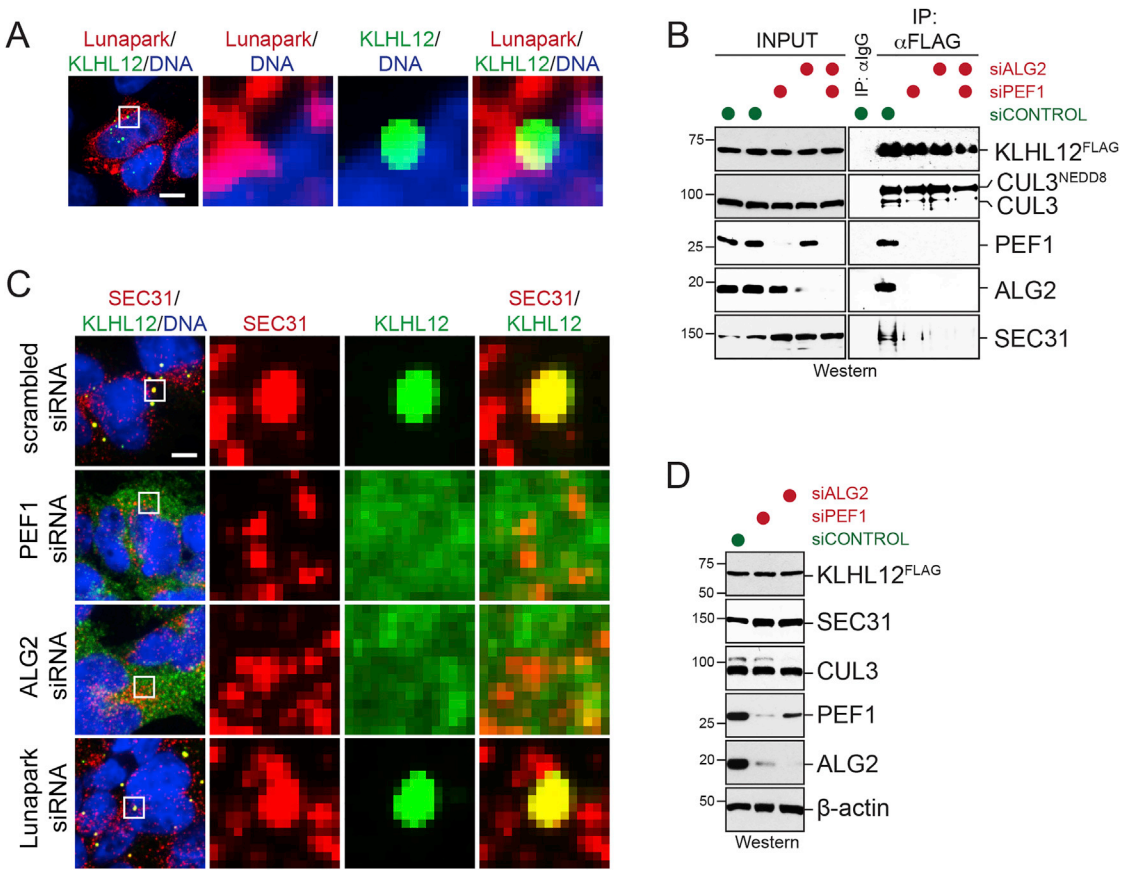

Figure S2. PEF1 and ALG2 Are Required for Substrate Binding by CUL3^{KLHL12}, Related to Figure 3

(A) Lunapark does not co-localize with KLHL12 on large COPII coats. Cells expressing both Lunapark^{HA} and KLHL12^{FLAG} were analyzed for protein localization using indirect immunofluorescence microscopy. The scale bar is 10 μm.

(B) PEF1 and ALG2 are required for substrate binding by CUL3^{KLHL12}. KLHL12^{FLAG}-expressing cells were transfected with control siRNAs or siRNAs targeting PEF1 or ALG2. KLHL12 was immunoprecipitated on αFLAG-agarose, and bound proteins were analyzed by western blotting.

(C) PEF1 and ALG2, but not Lunapark, are required for formation of large COPII coats. KLHL12-expressing cells were transfected with control siRNAs or siRNAs targeting PEF1, ALG2, or Lunapark and analyzed for SEC31 and KLHL12 co-localization by indirect immunofluorescence microscopy; scale bar is 10 μm.

(D) Expression control for KLHL12^{FLAG}-levels in cells transfected with either control siRNAs or siRNAs targeting PEF1 or ALG2. Protein levels were monitored by western blotting.

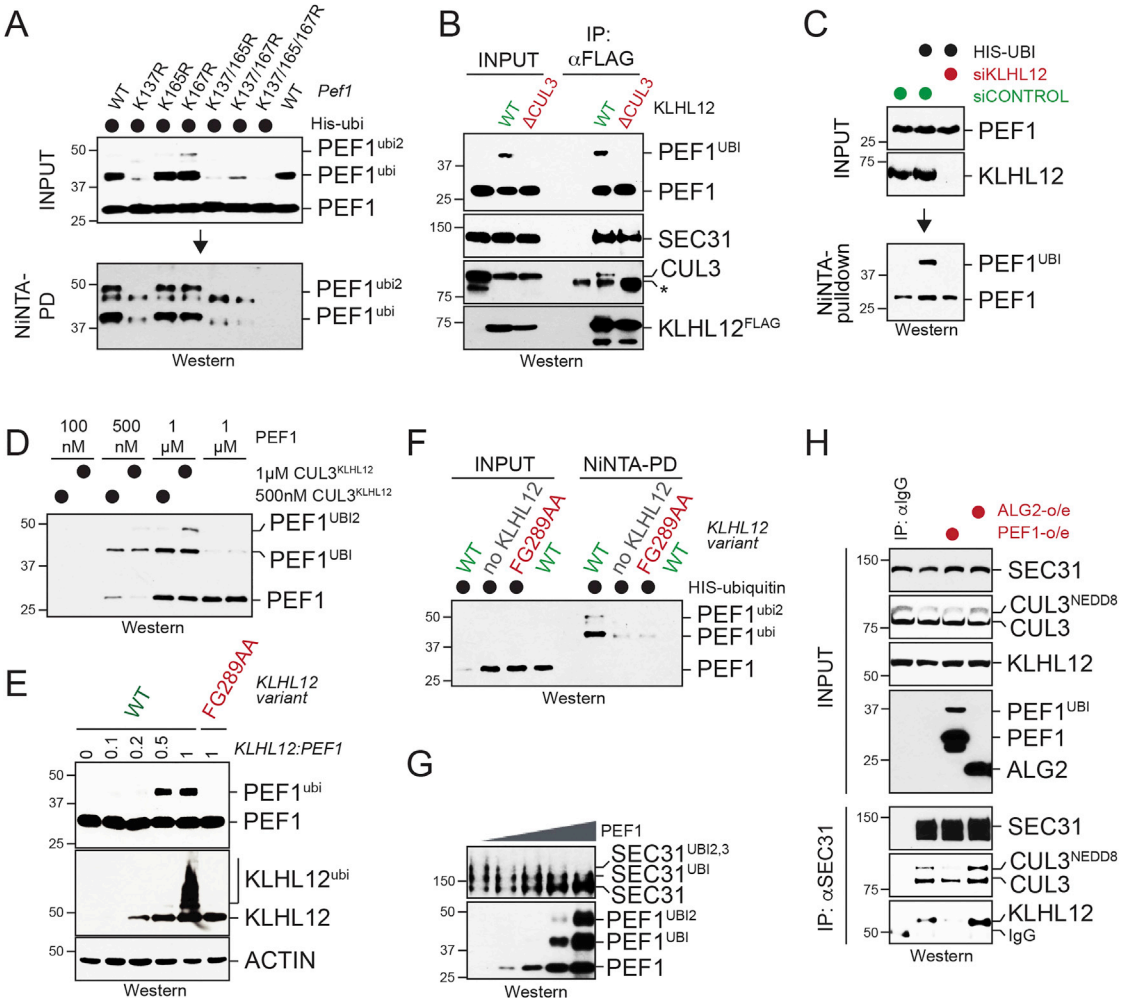

Figure S3. PEF1 Binds the Kelch Repeats of KLHL12, Related to Figure 4

(A) PEF1 is ubiquitylated in cells. PEF1 or variants of PEF1 with mutations in indicated Lys residues were expressed in cells that also produced ^{HIS}ubiquitin. Ubiquitylated proteins were purified under denaturing conditions on NiNTA agarose and analyzed for modified PEF1 by western blotting.

(B) CUL3^{KLHL12} ubiquitylates PEF1 in cells. FLAG-epitope-tagged KLHL12 or KLHL12$^{\Delta CUL3}$ (a variant unable to associate with CUL3) were affinity purified from human embryonic kidney cells and analyzed for bound proteins by western blotting. Expression of KLHL12, but not KLHL12$^{\Delta CUL3}$, induced monoubiquitylation of PEF1.

(C) Endogenous CUL3^{KLHL12} ubiquitylates endogenous PEF1. Cells expressing ^{HIS}ubiquitin were transfected with siRNAs targeting KLHL12. Ubiquitylated proteins were purified under denaturing conditions and tested for PEF1 modification by western blotting.

(D) CUL3^{KLHL12} ubiquitylates PEF1 in vitro. Increasing concentrations of recombinant PEF1 were incubated with either 0.5 μM or 1 μM recombinant CUL3^{KLHL12}, E1, UBE2D3, ubiquitin, and ATP. Ubiquitylation of PEF1 was analyzed by western blotting.

(E) CUL3^{KLHL12} ubiquitylates PEF1 in cells. Cells were transfected with increasing amounts of KLHL12 or substrate-binding-deficient KLHL12^{FG289AA}, and ubiquitylation of PEF1 was analyzed by western blotting.

(F) CUL3^{KLHL12} ubiquitylates PEF1 in cells. ^{HIS}ubiquitin-expressing cells were transfected with KLHL12 or substrate-binding-deficient KLHL12^{FG289AA}. Ubiquitylated proteins were purified under denaturing conditions over NiNTA agarose and analyzed for PEF1 by western blotting.

(G) PEF1 and SEC31 compete for access to KLHL12. In vitro ubiquitylation reactions of recombinant SEC31 (in complex with SEC13) were performed by CUL3^{KLHL12}, E1, UBE2D3, and ATP in the presence of increasing PEF1 concentrations. SEC31 and PEF1 ubiquitylation was detected by western blotting.

(H) SEC31 and PEF1 compete for access to KLHL12 in cells. Endogenous SEC31 was affinity purified from cells that overexpressed either PEF1 or ALG2, and bound CUL3^{KLHL12} was detected by western blotting.

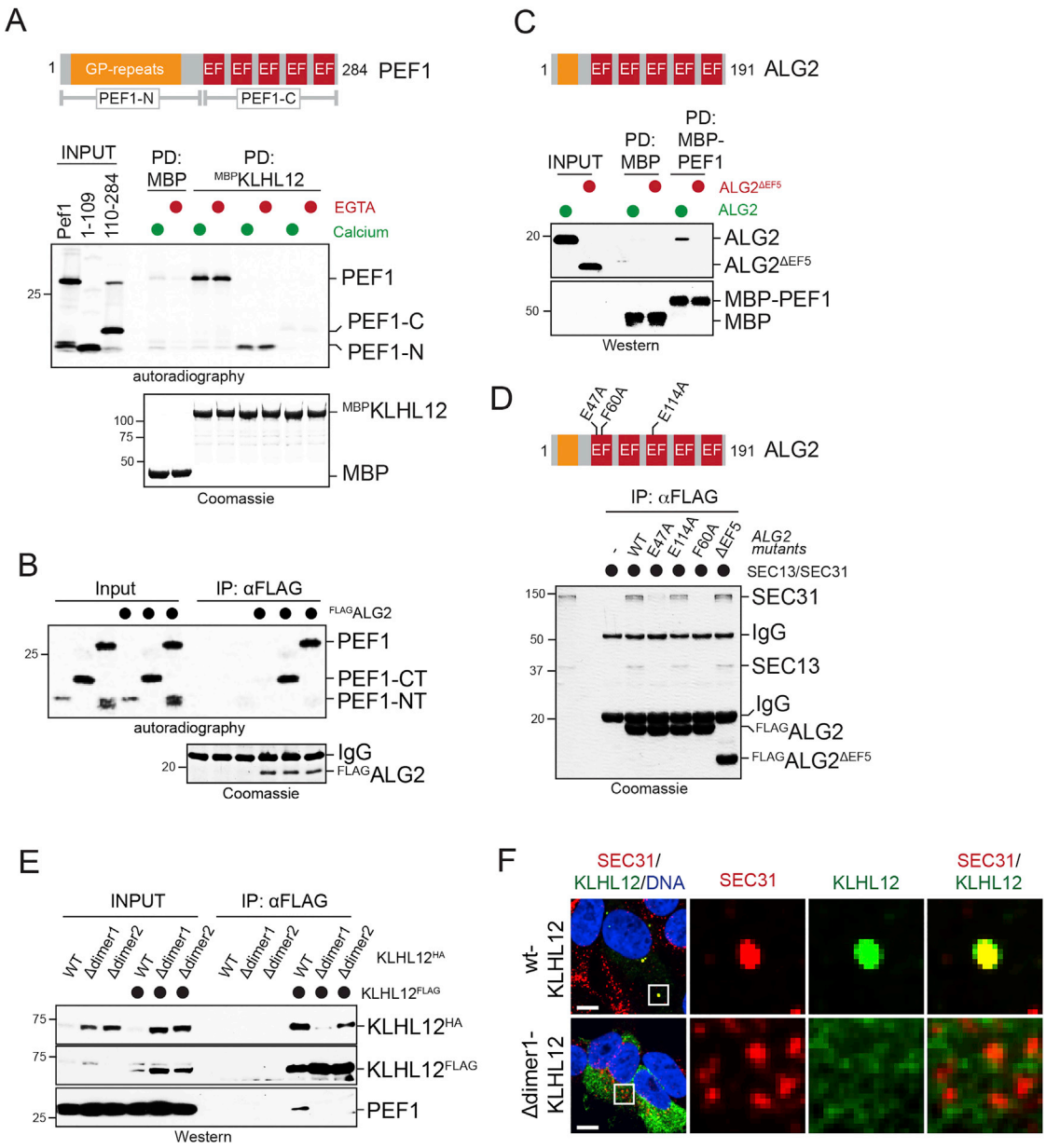

Figure S4. Architecture of the CUL3^{KLHL12}-PEF1-ALG2-SEC31 Complex, Related to Figure 4

(A) PEF1 binds KLHL12 through its amino-terminal Gly-Pro repeats. ^{35}S-labeled PEF1, N-PEF1 (i.e., Gly-Pro-rich repeats), or PEF1-C (EF-hand domains) were incubated with immobilized MBP or ^{MBP}KLHL12, respectively. Bound PEF1 proteins were detected by autoradiography.

(B) PEF1 binds ALG2 through its carboxy-terminal EF hand domain. ^{35}S-labeled PEF1 proteins (described above) were incubated with immobilized ^{FLAG}ALG2, and bound proteins were detected by autoradiography.

(C) ALG2 binds to PEF1 through its fifth EF hand. Recombinant ALG2 or ALG2$^{\Delta EF5}$ were incubated with immobilized MBP or ^{MBP}PEF1, respectively. Bound proteins were detected by western blotting.

(D) ALG2 binds SEC31 through its first EF hand. Recombinant SEC31 was incubated with immobilized WT ALG2 or variants of ALG2 with mutations in the first EF hand (E47A, F60), third EF hand (E114A), or fifth EF hand (ΔEF5). Bound proteins were detected by Coomassie staining.

(E) Identification of a dimerization-deficient KLHL12 mutant. Residues in the KLHL12 BTB interface were selected for mutagenesis based on previous work on the SPOP substrate adaptor (Zhuang et al., 2009). Mutations were introduced into KLHL12^{HA} and tested for dimerization with WT KLHL12^{FLAG}. Interactions were determined by αFLAG affinity purification and western blotting using HA, FLAG, or PEF1-antibodies.

(F) Dimerization-deficient KLHL12 fails to induce large COPII coat formation. WT or dimerization-deficient KLHL12 were expressed in human embryonic kidney cells and tested for formation of large SEC31-positive COPII structures by indirect immunofluorescence microscopy.

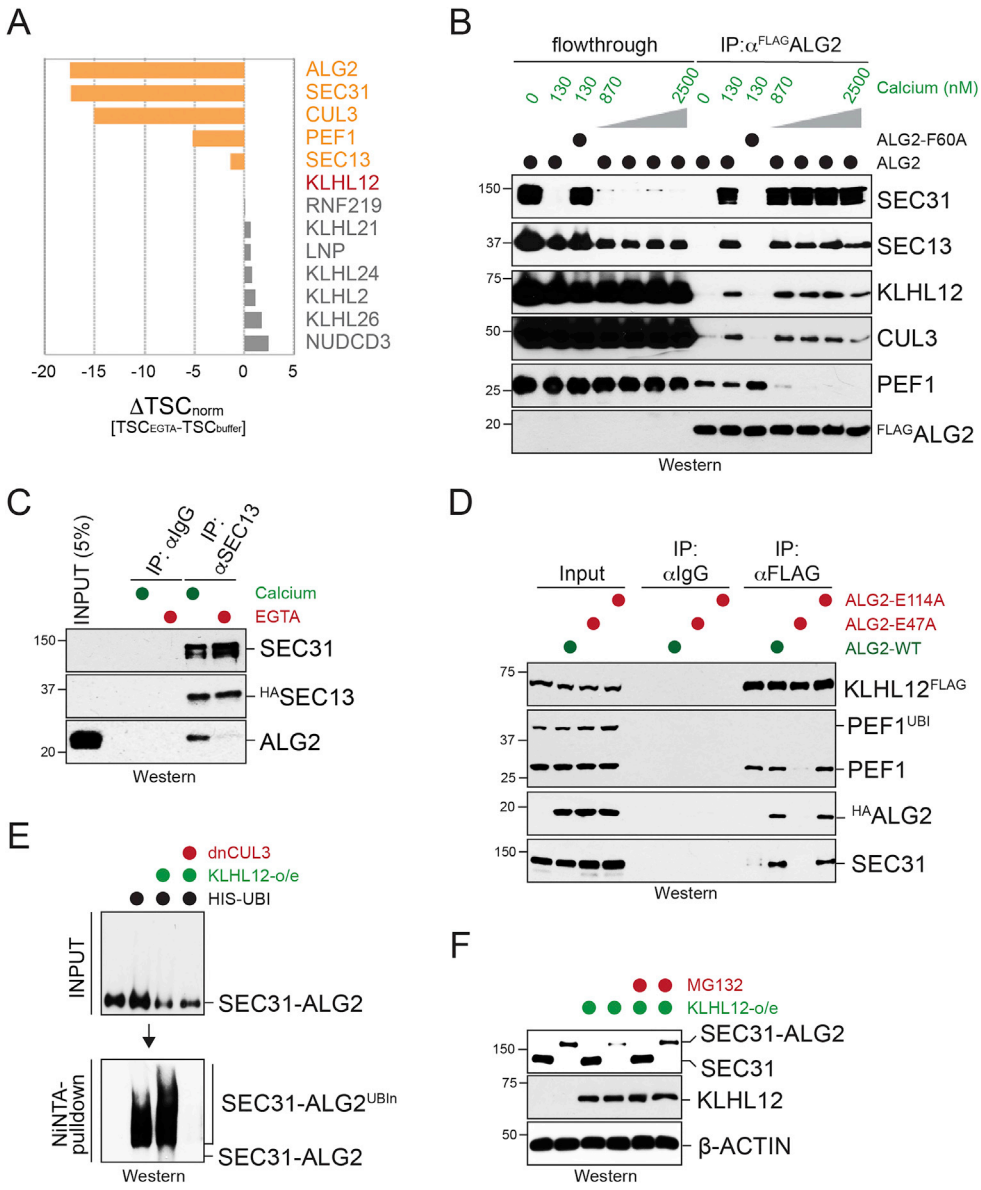

Figure S5. CUL3^{KLHL12} Is a Calcium-Dependent Ubiquitin Ligase, Related to Figure 5

(A) Calcium is required for SEC31 recognition by CUL3^{KLHL12}. Lysates of cells stably expressing KLHL12^{FLAG} under control of a doxycycline-inducible promoter were used to affinity purify KLHL12^{FLAG} both in the presence and absence of calcium (i.e., presence of EGTA), and bound proteins were determined by CompPASS mass spectrometry and total spectral counting.

(B) Physiologically relevant calcium concentrations regulate formation of CUL3^{KLHL12} complexes in vitro. ^{FLAG}ALG2 or ^{FLAG}ALG2^{F60A} (a calcium-signaling-deficient variant of ALG2) were immobilized on FLAG-agarose and incubated with the indicated proteins at either 10 mM EGTA, 130 nM calcium (to mimic the cellular concentration seen upon calcium release from the ER), or 800 nM calcium and above. Bound proteins were determined by western blotting.

(C) Chelation of calcium abrogates the interaction between SEC31 and ALG2. Recombinant SEC31 was immobilized on beads using αHA antibodies, incubated with ALG2, and analyzed for bound proteins by western blotting. Experiments were performed in the presence or absence (EGTA) of calcium.

(D) Calcium-binding-deficient ALG2^{E47A} disrupts formation of the CUL3^{KLHL12} ubiquitin ligase. KLHL12 was immunoprecipitated from control cells or from cells that overexpressed WT ALG2, ALG2^{E47A}, or ALG2^{E114A}. Bound proteins were detected by western blotting.

(E) CUL3^{KLHL12} ubiquitylates the SEC31-ALG2 fusion protein. The SEC31-ALG2 fusion was expressed in human embryonic kidney cells that also produced ^{HIS}ubiquitin. KLHL12 and dominant-negative CUL3$^{1–252}$ were expressed as indicated. Ubiquitylated proteins were purified under denaturing conditions over NiNTA agarose and analyzed for SEC31-ALG2 modification using western blotting.

(F) Polyubiquitylation of the SEC31-ALG2 fusion triggers its proteasomal degradation. Cells were transfected with SEC31, SEC31-ALG2, and KLHL12 as indicated. When noted, cells were treated with the proteasome inhibitor MG132, and protein levels were determined by western blotting.

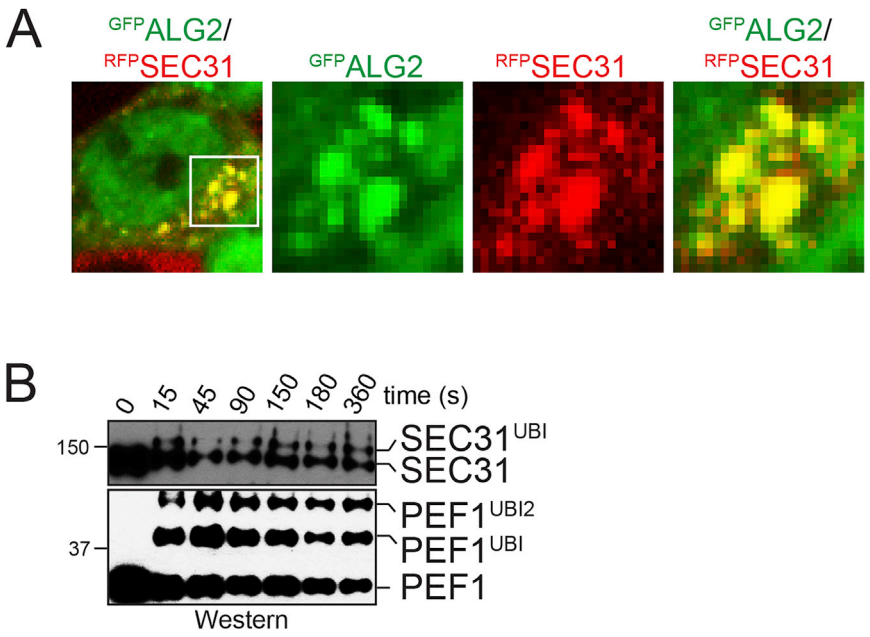

Figure S6. CUL3^{KLHL12} Is a Rapid Calcium-Dependent Ubiquitin Ligase, Related to Figure 7

(A) Calcium influx caused co-localization of ^{GFP}ALG2 and ^{RFP}SEC31. Representative cells depict localization 18 s after triggering calcium influx.

(B) CUL3^{KLHL12} ubiquitylates SEC31 and PEF1 very rapidly. Purified PEF1 and SEC31 were incubated with recombinant CUL3^{KLHL12}, ALG2, E1, UBE2D3, ubiquitin, and ATP and incubated at 30C for the indicated times. Ubiquitylation of SEC31 and PEF1 was analyzed by western blotting.